

Semiclassical study of intersubband cavity polaritons: Role of plasmonic and radiative coupling effects

M. Załuźny and W. Zietkowski

Institute of Physics M. Curie-Skłodowska University, Pl. M. Curie-Skłodowskiej 1, 20-031 Lublin, Poland

(Received 21 June 2012; revised manuscript received 28 May 2013; published 12 November 2013)

We theoretically discuss the properties of intersubband polaritons supported by a multiple-quantum-well structure embedded in the planar microcavity with dielectric and plasmonic mirrors. A semiclassical approach based on the transfer matrix formalism supplemented by the sheet model and the “microscopic” implementation of the effective medium approximation is employed. The presence of the intrasubband transition is taken into account. The obtained results show that in the case of realistic systems exhibiting superstrong coupling regime, radiative coupling between cavity modes can lead to the violation of a commonly used single-mode cavity approximation. It manifests itself as a formation of hybrid polariton modes having a non-negligible admixture of higher photonic modes and/or surface plasmonic modes. The comparison with results predicted by a microscopic quantum approach recently developed is also presented. Performing the above mentioned comparison we pay special attention to the role of intra- and interwell Coulomb couplings.

DOI: [10.1103/PhysRevB.88.195408](https://doi.org/10.1103/PhysRevB.88.195408)

PACS number(s): 78.67.Pt, 73.20.Mf, 78.20.Bh

I. INTRODUCTION

The linear intersubband response of multiple-quantum-well (MQW) structures embedded in planar microcavities (MCs) has been studied by many authors for both fundamental physics and application reasons. The coherent dipole coupling between the collective intersubband excitation having the frequency ω_{IT} and the ground photonic mode is usually characterized by the resonant Rabi coupling frequency Ω_R^{res} . In the strong-coupling regime, the above mentioned quantity dominates the decay rates of the intersubband excitation and the photonic mode. Due to this dominance, the formation of mixed modes termed intersubband-cavity-polaritons (ICPs) is possible. Such a type of modes, named the upper polariton branch (UPB) and lower polariton branch (LPB), were first observed in 2003 by two groups^{1,2} as a double-peak structure in the angle-resolved absorption spectra. The minimal frequency separation between the above mentioned polariton peaks ($\Delta_{\text{ICP}}^{\text{min}}$) is usually several times larger than the resonant Rabi splitting frequency in the momentum space ($\Delta_{\text{ICP}}^{\text{min}} \approx 2\Omega_R^{\text{res}}$). This difference is due to the fact that the absorption peaks are connected with ICP branches having different in-plane wave vectors.³⁻⁵

The largest value, for planar MQW-MC systems, of the normalized coupling frequency $\Omega_R^{\text{res}}/\omega_{IT} \approx 0.11$ was reported by Anappara *et al.*⁶ It is interesting to note that the larger values of the normalized coupling frequency have been realized using zero-dimensional metallic MCs⁷⁻⁹ and inductance-capacitance electronic microresonators.¹⁰

Since only the normal component of the electric field couples to the intersubband excitation, the experimentally studied planar semiconductor microcavities are designed to operate at a large angle of incidence $\varphi (\approx 70^\circ)$ with respect to the growth direction z . In the above mentioned limit, the frequency separation between the two lowest cavity (photonic) modes in the momentum space (Δ_{CM}) is several times smaller than ω_{IT} .^{4,5} It is not difficult to achieve the following experimental condition: $\Delta_{\text{ICP}}^{\text{min}} \gtrsim \Delta_{\text{CM}}$.^{3,6,11-14} In the literature, this regime is called the superstrong coupling (SSC) regime.¹⁵ When the SSC regime is achieved, more than one cavity

modes “see” and interact with the intersubband excitation. It gives rise to new physical effects not observed in systems exhibiting “ordinary” strong coupling regime. For example, the normal-mode splitting can occur for more than one cavity modes (therefore denoted as the multi-normal-mode splitting). It manifests itself as the formation of additional peaks in the absorption spectra. Such peaks have been observed experimentally by Dupont *et al.*^{2,14} in the MQW-MC system where the whole space between the mirrors is uniformly occupied by the QWs. We have shown⁵ that the above mentioned phenomena can be interpreted as diagonal coupling between “dark” intersubband states and higher photonic modes.

The behavior of the UPB and LPB is usually modeled employing a semiclassical approach based on the transfer matrix formalism⁵ (TMF) or the simplified multibeam interference analysis.¹⁶ The TMF is very convenient for the calculations of reflection and absorption spectra of MQW-MC systems. Moreover, taking the external field to be zero we can also obtain the dispersion relations for the electromagnetic modes of the systems.

The situation is different when we want to describe the luminescence process, which is closely related to the quantum nature of the ICPs.¹⁷⁻²¹ Then the approach based on the (simplified) coupled-harmonic-oscillator model^{5,22-24} is more suitable. However, the above mentioned oscillator model is based on the rotating wave approximation (RWA). Thus it does not work correctly when $2\Omega_R^{\text{res}}$ becomes a significant fraction ω_{IT} . This situation corresponds to the ultrastrong coupling (USC) regime. Note that the USC should be distinguished from the already mentioned superstrong coupling (SSC) regime referring to the scenario where polariton branch splitting $\Delta_{\text{ICP}}^{\text{min}}$ becomes comparable with the cavity mode separation Δ_{CM} . Thus, in the case of the typical semiconductor MCs, where Δ_{CM} is several times smaller than ω_{IT} , the USC regime is achieved at substantially larger value of the resonant Rabi frequency Ω_R^{res} than the SSC regime. It is obvious that in systems exhibiting the USC regime the already mentioned simplified oscillator model should be replaced by a more sophisticated microscopic quantum-mechanical approach,^{8,25-28}

which includes the non-RWA terms. The above mentioned terms not only substantially modify the ICP spectra but also lead to the appearance of new phenomena such as the generation of the correlated photon pairs.²⁵

Practically, in all the papers employing the quantum approach, as well as the simplified oscillator model the authors assume that the formation of the LPB and the UPB is connected with the coupling of the intersubband excitation with the ground photonic mode. It is the so-called single mode cavity approximation (SMCA). To our knowledge the range of validity of the above mentioned approximation has not been discussed in the literature so far. Semiclassical estimations reported in our recent paper⁵ (see also Ref. 29) indicate that the SMCA has a good justification when the system is uniform, i.e., when the mirrors are perfect and the whole space between mirrors is occupied by the MQW slab. If these conditions are not fulfilled, the radiative coupling between the cavity modes should be considered in the systems exhibiting the SSC regime. The above mentioned coupling manifests itself as the formation of the LPB and the UPB with a non-negligible admixture of higher cavity modes.

Discussing the validity of the SMCA we should also take into account the fact that in many systems experimentally studied the n -doped dielectric layers (or multilayers) also play the role of one^{3,6} or both^{2,14} of the MC mirrors. The presence of free carriers in the mirror material leads to the reduction of the real part of the mirror dielectric function [$\epsilon_{\text{mirr}}(\omega)$]. Because of that, the plasmonic mirrors can be much thinner compared to purely dielectric mirrors. They also allow for the electrical pumping of the MQW-MC systems. However, the presence of free electrons in the mirror material not only affects the dispersion characteristics of the photonic modes but also leads to the formation of additional - surface plasmon polariton (SPP) modes. The above mentioned modes are located below the ground photonic mode or, more precisely, below the plasma frequency ($\omega_{p,\text{mirr}}$) of the mirrors.³⁰⁻³² It is obvious that the formation of the ICP branches with a non-negligible admixture of the SPP modes cannot be excluded *a priori* in the case of the systems where $\omega_{p,\text{mirr}}$ is comparable with ω_{IT} .

It is well known that the intrasubband collective modes are also supported by the MQW slab.^{30,33} These modes are located below the plasma frequency (ω_p) of the bulk MQW. In the case of symmetric QWs the direct interaction between intrasubband and intersubband plasmons is forbidden.³⁴ Nevertheless, when the MQW is located inside the semiconductor MC, the interaction through cavity photons²² becomes possible. In other words, the violation of the SMCA is potentially possible due to the formation of the mixed hybrid ICP branches with an admixture of the intrasubband plasmonic mode. At this point, we would like to stress that the phenomena connected with the formation of the intrasubband plasmon have been recently discussed,^{30,35-37} but not in the context of their influence on the ICP characteristics.

The aim of this work is to provide a systematic analysis of the dispersion characteristics of the UPB and the LPB supported by planar MQW-MC systems. Special attention will be paid to the plasmonic and radiative coupling effects leading to the violation of the SMCA. Such an analysis seems to be extremely relevant in the light of recent achievements in

the construction of new electroluminescent devices based on ICPs.¹⁸⁻²¹

We employ a semiclassical approach based on the TMF supplemented by the “microscopic” effective medium approximation and the so-called sheet model.^{5,38} To clearly understand the origin of the considered phenomena properly simplified Fabry-Perot models are also considered. A great advantage of the simplified models is that the polariton characteristics predicted by them can be directly compared with those obtained employing the microscopic quantum electrodynamics.^{7,26,27} They also allow for the demonstration of the important role of the interwell Coulomb coupling^{4,33} in systems exhibiting the USC.

The theoretical background is presented in Sec. II. Simplified analytical calculations are performed in Sec. III. In Sec. IV, the numerical results obtained with the help of the TMF for parameters corresponding to realistic systems with dielectric and plasmonic mirrors are reported and discussed. Section V is a brief conclusion. Some technical details are presented in Appendices A–H. The acronyms and main symbols introduced in this paper are listed in Appendix I for the reader’s convenience.

II. THEORETICAL BACKGROUND

A. Transfer matrix formalism and electromagnetic eigenmodes

The planar MQW-MC system can be, in general, treated as a layered structure sandwiched between the nonabsorptive semi-infinite substrate ($j = 0$) and cladding ($j = m$) media with the dielectric constants $\epsilon_0 = \epsilon_s$ and $\epsilon_m = \epsilon_c$, respectively. Consider a harmonic plane wave (polarized in the x - z plane) with an $\exp(-i\omega t)$ temporal dependence incoming on the stack from the substrate at the angle φ . The relation between the (complex) amplitudes of the magnetic field in the substrate and cladding media is determined by the 2×2 transfer matrix of the system \mathbf{T} .³⁸ The above matrix can be considered as a product of matrices \mathbf{L}_j and $\mathbf{I}_{j,j+1}$. The matrix \mathbf{L}_j describes the effect of propagation through the j th layer, while the matrix $\mathbf{I}_{j,j+1}$ accounts for the interface between layers j and $j + 1$.

Unfortunately, the calculation of the transfer matrix across the MQW is a rather complex problem. The intersubband and intrasubband optical response of the infinite MQW has been discussed by King-Smith and Inkson³⁹ employing a semiclassical self-consistent approach based on the Coulomb-gauge minimal-coupling Hamiltonian. The same Hamiltonian has been used in the work by Liu⁴⁰ devoted to the intersubband response of the MQW embedded into semiconductor MC. Unfortunately, the formalism used by Liu is very complex and practically not amenable to some analytical treatment. Moreover, the author takes into account only the paramagnetic contribution in the intersubband response (see Appendices A and B). Because of the above mentioned simplification, the approach employed by Liu is not appropriate for the study of systems exhibiting the USC regime.

In order to overcome the difficulty, we employ the fact that the effective thickness of the QW is much smaller than the wavelength of the radiation interacting with intersubband excitation [the long-wavelength approximation (LWA)]. Thus we can work in the dipole gauge Hamiltonian.⁴¹⁻⁴³ It is also

reasonable to assume that the quasi-2D-electron gas (Q2DEG) located in the QW, can be considered as an infinitely thin sheet (centrally positioned in the QW) carrying a field-induced current.^{38,41,44} It is a so-called sheet model. Since we employ the semiclassical approach, the current induced in the QW has to be determined in a self-consistent manner.⁴³ The sheet conductivity (σ_{zz}) describing the linear intersubband response to the z component of the external (not total) electric field is given in Appendix A.

Usually, the MQW slab contains a large number of QWs ($N_{\text{QW}} \gg 1$). Moreover, the spatial period of the MQW (d_{MQW}) is much smaller than the wavelength of the incident radiation. It means that in the case of typical systems the homogenization of the sheet model is possible. In other words, the sheet model can be replaced by a much more convenient for analytical and numerical calculations “microscopic” implementation of the effective medium approximation (EMA).³⁸ An important advantage of this approximation is that the intrasubband excitation can be simply incorporated introducing (see Appendix A) the intrasubband sheet conductivity (σ_{xx}).

In the considered approximation, the MQW is treated as a uniform uniaxial medium (slab) with the diagonal effective dielectric tensor $\varepsilon_{\rho\rho'} = \delta_{\rho\rho'} \varepsilon_{\rho\rho}$ ($\rho, \rho' = x, y, z$).³⁸ The relations between the principal components $\varepsilon_{xx} = \varepsilon_{yy}$ and ε_{zz} of the effective dielectric tensor and the intrasubband σ_{xx} and the intersubband σ_{zz} components of the sheet conductivity tensor are given in Appendix A.

The complex reflection coefficient of the MQW-MC structure (r) is connected with the elements of the corresponding transfer matrix \mathbf{T} by the relation $r = T_{21}/T_{11}$. We concentrate on a typical situation when the transmission through the back mirror can be taken as zero. Then, the absorptance (equal to the fraction of the incident energy absorbed) of the structure is given by $A = 1 - |r|^2$.

The characteristic equation for electromagnetic modes supported by the system, resulting from the requirement that no light incidents on the cavity from outside, takes the form

$$T_{11} = 0. \quad (1)$$

The above mentioned modes can be generally divided into two classes: (i) nonradiative (bound) modes and (ii) radiative (virtual) modes. We concentrate on the constant-angle virtual modes, which are accessible by angle resolved reflectance-absorptance measurements. They radiate the energy into the substrate at the fixed and real angle φ . The above mentioned facts imply that not only the frequency of the κ th constant-angle virtual mode but also its in-plane wave vector should be treated as complex-valued quantities, $\tilde{\omega}_\kappa = \omega'_\kappa + i\omega''_\kappa$ and $\tilde{k}_{\kappa,x} = k'_{\kappa,x} + ik''_{\kappa,x}$, satisfying the relation $\tilde{k}_{\kappa,x}/\tilde{\omega}_\kappa = |\tilde{k}_{\kappa,x}/\tilde{\omega}_\kappa| = (\varepsilon_s^{1/2}/c) \sin \varphi$. The details can be found in Ref. 45 (see also Ref. 46).

Let us assume that the frequency of the κ th radiative mode is spectrally separated from the rest of the modes. Then such a mode can be associated with a Lorentzian shape maximum in the angle-resolved absorptance of width $2\gamma_\kappa = -2\omega''_\kappa$ centered at ω'_κ .^{5,45} The mode is treated as a well defined entity only when $|\omega''_\kappa| \ll \omega'_\kappa$. In this limit, a dispersion relation for the polaritons in terms of frequency versus in-plane wave vector (more precisely the real part of the above mentioned vector)

can be extracted from the angle-resolved dispersion using the following relation:

$$k_x \equiv k'_{\kappa,x} \cong (\varepsilon_s^{1/2}/c) \omega'_\kappa(\varphi) \sin \varphi. \quad (2)$$

B. Characteristic equations for simplified models

1. Basic formula

For our purpose, it is very convenient to have the dispersion equations for electromagnetic modes, which are explicitly written in terms of the coefficients associated with the light reflection by the Q2DEG. We derive such equations for the MQW-MC system and for the system consisting of a single QW embedded into the MC.

Let us denote by \mathbf{T}^{cb} the transfer matrix from the coupling (c) to the back (b) mirror. The condition that only outgoing waves exist outside the system implies the following matrix equation for the eigenfrequency:

$$\mathcal{G} \begin{bmatrix} r_c \\ 1 \end{bmatrix} = \mathbf{T}^{\text{cb}} \begin{bmatrix} 1 \\ r_b \end{bmatrix}, \quad (3)$$

where r_c (r_b) is the reflection coefficient of the coupling (back) mirror.

We assume for convenience that the spacer layers, with the dielectric constant ε_{sl} , are placed between the MQW slab (or the single QW) and the mirrors. It implies that the reflection coefficients r_c and r_b correspond to the situation when the light incidents from the medium with the dielectric constant ε_{sl} .

Eliminating coefficient \mathcal{G} from Eq. (3), one gets

$$T_{11}^{\text{cb}} + T_{12}^{\text{cb}} r_b = r_c (T_{21}^{\text{cb}} + T_{22}^{\text{cb}} r_b). \quad (4)$$

In further discussion, we neglect for simplicity the dielectric mismatch. More precisely, we neglect the differences between the dielectric constants of the spacer layer(s) (ε_{sl}), the substrate (ε_s), the barrier (ε_b) and the well (ε_w) materials taking $\varepsilon_{\text{sl}} = \varepsilon_s = \varepsilon_b = \varepsilon_w$. The above mentioned approximation modifies the resonance conditions between the intersubband excitation and the ground photonic mode. Nevertheless, it does not affect the main conclusions resulting from simplified models considered in the next section. We would like to stress that the numerical results reported in Sec. IV have been obtained taking into account the dielectric mismatch.

2. The MQW-MC system

Now we apply Eq. (4) to the MQW-MC system in which the thicknesses of the spacer layers are negligibly small compared to mirror separation (L_{MC}), i.e., the cavity thickness. In other words, we assume that L_{MC} practically coincides with the thickness of the MQW slab (L_{MQW}). (Note that in Ref. 26 the thickness of the MQW slab is denoted by L_{QW} .) In the system of interest here, the matrix \mathbf{T}^{cb} , appearing in Eq. (3), can be written as a product³⁸ (see Appendix C1):

$$\mathbf{T}^{\text{cb}} \cong \mathbf{I}(r_{\text{MQW}}) \mathbf{L}(\beta_{\text{MQW}}/2) \mathbf{I}(r_{\text{MQW}}), \quad (5)$$

where $\beta_{\text{MQW}} = k_{\text{MQW},z} L_{\text{MQW}}$ and

$$k_{\text{MQW},z} = [\varepsilon_{xx} (K^2 - k_x^2 / \varepsilon_{zz})]^{1/2} \quad (6)$$

is the z component of the wave vector in the MQW slab. ($K = \omega/c$ is the wave vector of the radiation in vacuum and c is

the speed of light in vacuum.) Moreover, r_{MQW} is the reflection coefficient associated with the interface between the semi-infinite MQW and the medium with dielectric constant ε_w (the MQW- ε_w interface). Light incidents from the dielectric.

Substituting the expressions for the components of \mathbf{T}^{cb} given by Eqs. (C5)–(C7) into (4), we get the characteristic equation for the system:

$$1 - r_c r_b e^{i2\beta_{\text{MQW}}} = -r_{\text{MQW}}(r_b + r_c)(1 - e^{i2\beta_{\text{MQW}}}) + r_{\text{MQW}}^2(1 - r_c r_b)e^{i2\beta_{\text{MQW}}}. \quad (7)$$

Let us assume that $r_{\text{MQW}} \rightarrow 0$. It means that we completely neglect the effects introduced by the optical interference between the light reflected from the MQW- ε_w interfaces and the light reflected from the cavity mirrors. In this limit, Eq. (7) simplifies to the form consistent with the multibeam interference analysis¹⁶

$$1 - r_c r_b e^{i2\beta_{\text{MQW}}} = 0. \quad (8)$$

One can check that in the case of the systems with identical perfect mirrors ($r_c = r_b$ and $|r_c| = |r_b| = 1$) characteristic equation (7) reduces to the form

$$1 - e^{i2\beta_{\text{MQW}}} = 0, \quad (9)$$

which is not affected by the above mentioned interference.

The inspection of Eqs. (7) and (9) shows that the effects connected with the light reflection by the Q2DEG start to play an important role when the cavity modes substantially penetrate into the mirrors or more precisely, when the effective thickness of the MC (see Sec. III B) is substantially larger than the thickness of the MQW slab. In such systems, the optical interferences between the light reflected from the MQW- ε_w interfaces and the light reflected from the cavity mirrors modify the spatial variation of the LPB and the UPB compared to the spatial variation of the ground cavity mode. As mentioned in Introduction, it can be interpreted as a formation of the LPB and the UPB with a different admixture of higher photonic modes.⁴⁷ Equivalently, we can speak about the (radiative) coupling between the cavity modes mediated by the intersubband excitation.²⁹

3. The MC with a single QW

Now we discuss a strongly nonuniform case when a single QW is positioned centrally between the mirrors. For convenience, we neglect the intrasubband excitation. Modeling the Q2DEG by the 2D sheet we find that the transfer matrix across the cavity can be written as³⁸ (see also Appendix C2)

$$\mathbf{T}^{\text{cb}} = \mathbf{L}(\beta_{\text{MC}}/2)\mathbf{I}^{2\text{D}}\mathbf{L}(\beta_{\text{MC}}/2), \quad (10)$$

where $\beta_{\text{MC}} = k_{w,z}L_{\text{MC}}$, $k_{w,z} = (K_w^2 - k_x^2)^{1/2}$ and $K_w^2 \equiv \varepsilon_w K^2 = \varepsilon_w \omega^2/c^2$. Matrix $\mathbf{I}^{2\text{D}}$ corresponds to the 2D sheet embedded in a medium with dielectric constant ε_w . It can be written in terms of the transmission (t_{QW}) and reflection (r_{QW}) coefficients of the Q2DEG. The explicit form of \mathbf{T}^{cb} is presented in Appendix C2.

Let us assume for simplicity that $r_c = r_b$. Then, from Eqs. (4), (10), and (C11)–(C13), one finds the following

characteristic equation for the considered system:

$$0 = [r_c(t_{\text{QW}} + r_{\text{QW}})e^{i\beta_{\text{MC}}} - 1] \times [r_c(t_{\text{QW}} - r_{\text{QW}})e^{i\beta_{\text{MC}}} + 1]. \quad (11)$$

Deriving the above equation we have assumed that only a single QW is located inside the MC. Nevertheless, it is reasonable to expect that Eq. (11) can be also employed for the qualitative analysis of the role of radiative coupling effects, associated with spatial nonuniformity of systems, even when $N_{\text{QW}} > 1$.

III. ANALYTICAL SOLUTIONS FOR SIMPLIFIED MODELS

The solution of the “exact” dispersion equation (1) or even simplified equations (8) and (11) requires, in general, complicated numerical calculations. Unfortunately, they cannot provide an intuitive insight into the relations between various parameters. Accordingly, the analytical description is investigated and presented below. We discuss three simplified models employing formulas derived in Sec. II B.

A. Models with perfect mirrors

For a deeper insight into the polariton physics in the SSC regime and beyond, we model the realistic system by a simple (symmetric) Fabry-Perot resonator with perfect mirrors separated by the distance L_{MC} . The ohmic losses and dielectric mismatch are omitted for simplicity. We discuss two particular configurations corresponding to the uniform (model I) and strongly nonuniform (model II) systems.

Model I is composed of an MQW slab (with the thickness $L_{\text{MQW}} \cong L_{\text{MC}}$) bounded by perfect mirrors (see insert in Fig. 1). The coupling of the photonic modes with intersubband as well with intrasubband excitations is considered. In particular, we employ this model for the study of the influence of the intra- and interwell Coulomb coupling (see Appendix D) on the LPB and UPB characteristics.

Model II corresponds to the case when only a single QW, modeled by the 2D sheet, is centrally positioned between mirrors (see insert in Fig. 2). Such a configuration is appropriate for modeling of the MQW-MC systems with a small number of QWs ($L_{\text{MQW}} \ll L_{\text{MC}}$). With the help of this model we explicitly demonstrate the violation of the SMCA in the case of the nonuniform systems exhibiting the SSC regime.

We concentrate on the study of the k_x -dependent characteristics. The φ -dependent characteristics, predicted by model I, are very briefly discussed in Appendix E.

1. Model I

a. Basic formula and coupling selection rules. The characteristic equation (9) corresponding to the uniform system (model I) leads to a well known condition for the allowed values of $k_{\text{MQW},z}$:

$$k_{\text{MQW},z} = n\pi/L_{\text{MC}}. \quad (12)$$

The mode index n gives the number of half-wavelength of the standing waves of the mode-field across the MC. In the case of the metallic (dielectric) mirrors, $n = 0, 1, 2, \dots$ ($n = 1, 2, 3, \dots$). In further discussion, it is convenient to introduce

mirror type dependent parameter n_{\min} . The above mentioned parameter corresponds to the ground photonic mode index, i.e., it takes the value 0 (1) when mirrors are of a metallic (dielectric) type. In the case of the undoped (passive) MQW, the left-hand side of Eq. (12) should be replaced by $k_{w,z} = (\varepsilon_w K^2 - k_x^2)^{1/2}$.

The condition (12), supplemented by Eqs. (6) and (A5)–(A8) gives the following eigenvalue equation for the n th-order (hybrid) polariton branches:

$$\omega^2 - \varpi_n^2 = \frac{f_{12}\omega_p^2\omega_{\parallel}^2}{\omega^2 - \omega_{\Gamma}^2} + \frac{\omega_p^2 n^2 \omega_{\perp}^2}{\omega^2 - \omega_p^2}, \quad (13)$$

where $\omega_{\parallel}(k_x) = k_x c / \sqrt{\varepsilon_w}$, $\omega_{\perp} = \pi c / \sqrt{\varepsilon_w} L_{MC}$, $\varpi_n(k_x) = [\omega_{\parallel}^2(k_x) + (n\omega_{\perp})^2]^{1/2}$ is the (k_x -dependent) frequency of the n th-order photonic mode of the passive MQW-MC system, N_s is the surface concentration of the Q2DEG, $\omega_p = (4\pi N_s e^2 / d_{MQW} m^* \varepsilon_w)^{1/2}$ is the plasma frequency of the bulk MQW with the period d_{MQW} , m^* is the effective mass of the electron and f_{12} is the oscillator strength of the $1 \rightarrow 2$ transition. Moreover, $\omega_{\Gamma} = (\omega_{21}^2 + \omega_p^2)^{1/2}$ is the depolarization shifted intersubband resonant frequency, ω_{21} is the intersubband separation frequency and $\omega_p = \omega_p (d_{MQW} / L_{QW}^{\text{eff}})^{1/2}$ is the QW plasma frequency. The effective thickness of the quantum well (L_{QW}^{eff}) is defined in Appendix A. We assume that only ground subband is occupied. Note that Eq. (13) is valid when the restrictions imposed by the LWA are fulfilled, i.e., when $k_x d_{MQW} \ll 1$ and $k_{MQW,z} d_{MQW} = \pi n / N_{QW} \ll 1$.³⁹

It is obvious that if the size-quantization of $k_{MQW,z}$ is omitted, the solutions of Eqs. (6) and (A5)–(A8) describe the polariton branches supported by an infinite MQW. Their characteristics practically coincide (in the LWA) with the characteristics predicted by a much more sophisticated current-response theory based on the Coulomb-gauge minimal-coupling Hamiltonian.³⁹ The above mentioned coincidence supports the validity of the “microscopic” EMA, even if the presence of the intrasubband transitions is taken into account.

At this point it is worth recalling that the minimal-coupling Hamiltonian contains the intra- and interwell (nonretarded) Coulomb interactions.^{43,51} It is well known that in infinite MQWs the interwell Coulomb coupling leads to the delocalization of the intersubband and intrasubband plasmon modes associated with each QW. Equivalently, we can speak about the formation of the intersubband and intrasubband plasmon bands.³³ Since the MQW slab is bounded by perfect mirrors, the above modes are size quantized according to Eq. (12). In other words they can be labeled by the mode index n .

We denoted the quantized intersubband (intrasubband) Coulomb modes supported by the uniform MQW-MC systems by C_n^{inter} (C_n^{intra}). Making in Eq. (13) the substitution $c \rightarrow \infty$, one finds the following expressions for the frequencies of the above mentioned modes:

$$\omega_{C_n^{\text{inter}}} = \sqrt{\omega_{21}^2 + \omega_p^2 (1 - F \sin^2 \theta_n)}, \quad (14)$$

$$\omega_{C_n^{\text{intra}}} = \omega_p \sin \theta_n, \quad (15)$$

where $\sin \theta_n = k_x / [k_x^2 + (n\pi / L_{MC})^2]^{1/2} = \omega_{\parallel} / \varpi_n$ and

$$F = f_{12}(\omega_p / \omega_p)^2 = f_{12} L_{QW}^{\text{eff}} / d_{MQW}. \quad (16)$$

The system with perfect dielectric mirrors supports the intersubband and intrasubband Coulomb modes with mode index $n = 1, 2, 3, \dots$. In systems with perfect metallic mirrors, the intersubband Coulomb mode with index $n = 0$ can be additionally supported.

The above considerations (see also Appendix D and Ref. 43) lead to the following conclusion. When we work in the framework of the minimal-coupling Hamiltonian, the polariton branches, described by the eigenvalue equation (13), appear due to the coupling of the pure photonic mode with the intersubband as well as with the intrasubband Coulomb modes described by Eqs. (14) and (15), respectively.

It is important to stress that in the case of the uniform systems only the photonic and Coulomb modes having the same mode index are coupled. Thus we can speak about the diagonal coupling. This finding is consistent with the statement that in the above mentioned systems the photonic and Coulomb modes having the same mode index have the same oscillatory spatial dependence in the MC.

It is obvious that the nonuniformity of the MQW-MC system implies the different quantization conditions on the radiation and the material excitations. Consequently, in such systems we can expect an interaction between the Coulomb and cavity modes having different mode indexes (nondiagonal coupling). Equivalently, we can speak about the radiative coupling between the cavity modes induced by the intersubband excitation.²⁹ Note that the interpretation of the coupling selection rules presented above, in contrast with the interpretation based on the concept of the “bright” and “dark” states (see Ref. 5), takes into account the interwell Coulomb coupling and goes beyond the RWA.

b. Intersubband cavity polaritons. Initially, we shall ignore the intrasubband transitions ($\varepsilon_{xx} = \varepsilon_w$). In other words, we omit the second term on the right-hand side of Eq. (13). The above mentioned simplification has a good justification when $\omega_{\Gamma}^2, \omega^2 \gg \omega_p^2$. In this limit, Eq. (13) reduces to the form

$$(\omega^2 - \omega_{\Gamma}^2)(\omega^2 - \varpi_n^2) = 4\omega_{\Gamma}\varpi_n\Omega_{R,n}^2, \quad (17)$$

where $\Omega_{R,n} = (\omega_p/2)(F\varpi_n/\omega_{\Gamma})^{1/2} \sin \theta_n$.

Solving this equation, we get

$$\omega_{\pm,n}^2 = \frac{\omega_{\Gamma}^2 + \varpi_n^2}{2} \pm \sqrt{\frac{(\omega_{\Gamma}^2 - \varpi_n^2)^2}{4} + F\omega_p^2\omega_{\parallel}^2}. \quad (18)$$

The branches predicted by the above equation can be divided into the “resonant,” with $n \leq n^*$, and the “nonresonant,” with $n > n^*$, where n^* is the maximal value of n for which the condition $\varpi_n(k_x = 0) = n\omega_{\perp} \leq \omega_{\Gamma}$ is fulfilled. One can check that the n th-order resonant branch of the upper type ($+, n < n^*$) starts at $\omega = \omega_{\Gamma}$ and approaches ϖ_n as k_x increases. On the other hand, the n th-order resonant branch of the lower type ($-, n < n^*$) starts at $\omega = n\omega_{\perp}$ and approaches asymptotically the frequency $\bar{\omega}_{\Gamma} = (\omega_{\Gamma}^2 - \omega_p^2 F)^{1/2}$ as k_x increases. It is not an unexpected result since $\bar{\omega}_{\Gamma}$ coincides with $\omega_{C_n^{\text{inter}}}(k_x \rightarrow \infty)$ [see Eq. (14)]. Thus, in agreement with Refs. 26 and 10, model I predicts the formation of the polariton gap between ω_{Γ} and $\bar{\omega}_{\Gamma}$. The above mentioned phenomenon is directly related to the formation of the intersubband plasmon bands due to the interwell Coulomb coupling [see Eq. (14) and Appendix D]. It is worth stressing that the polariton gap

appears only for the resonant modes. As shown in Ref. 5, the nonresonant lower type branches ($-n > n^*$) are located in the above mentioned gap. They start at $\omega = \omega_{IT}$ and approach asymptotically $\bar{\omega}_{IT}$. It means that the in-gap polariton branches are well-modeled by the intersubband Coulomb modes described by Eq. (14).

At this point, we would like to note that the formation of in-gap polariton states is also demonstrated for a planar MC having all the space between the mirrors continuously filled by GaAs.⁴⁸ In such a system, the formation of the in-gap states is associated with the (diagonal) coupling of the higher photonic modes with excitonic states appearing due to the size-quantization of the exciton center-of-mass motion.⁴⁹

Note that the formula (17) has the same form as the (exact) eigenvalue equation describing two harmonic oscillators with the frequencies ω_{IT} and ϖ_n . The coupling between them is controlled by the frequency $\Omega_{R,n}$.⁵⁰ When we restrict to the SMCA ($n = n_{\min}$) then, in agreement with the quantum-mechanical approach developed in Ref. 26, the quantity $\Omega_{R,n_{\min}}$ can be treated as the (dipolar gauge) Rabi frequency determining the coupling between intersubband excitation and the ground cavity mode. In further discussion, the superscript n_{\min} in the SMCA Rabi frequency will be dropped for convenience, i.e., $\Omega_R \equiv \Omega_{R,n_{\min}}$.

The resonant Rabi frequency, introduced in Introduction, can be defined by $\Omega_R^{\text{res}} = \Omega_R(k_x^{\text{res}})$ where k_x^{res} is the resonant in-plane wave vector such that $\varpi_{n_{\min}}(k_x) = \omega_{IT}$. Consequently, $\Omega_R^{\text{res}} = (\omega_p/2)F^{-1/2}$ in the case of the metallic mirrors and $\Omega_R^{\text{res}} = (\omega_p/2)F^{-1/2} \sin \theta_{\text{res}}$, with $\theta_{\text{res}} = \theta_1(k_x = k_x^{\text{res}})$, in the case of the dielectric mirrors.

We would like to stress that the above statement is consistent with the fact that in the dipolar gauge Hamiltonian there are no direct Coulomb interactions between QWs; instead they are mediated by an exchange of photons. In the minimal coupling Hamiltonian, the direct and image parts of the Coulomb interactions are explicitly present.^{43,51}

Let us assume that $\omega_p^2 \ll \omega_{21}^2$ and $k_x \approx k_x^{\text{res}}$. In the above mentioned limit, Eq. (17) can be approximated and recast (for the UPB and the LPB) in the eigenvalue equation predicted by the simplified oscillator model

$$(\omega - \omega_{IT})(\omega - \varpi_{n_{\min}}) = (\Omega_R^{\text{res}})^2. \quad (19)$$

Figure 1 presents numerical solutions of the ‘‘exact’’ equation (13) (solid curves), the SMCA equation (17) in which the intrasubband excitation is omitted (gray spheres) and the two-oscillator equation (19) (crosses), for a uniform system with dielectric mirrors ($n_{\min} = 1$). The numerical values used for solving the above mentioned equations are $\omega_p = 0.4 \omega_{IT}$, $f_{12} = 0.86$, and $\omega_{\perp} = 0.4 \omega_{IT}$. It corresponds to $n^* = 2$, $\theta_{\text{res}} = 68^\circ$, and $\bar{\omega}_{IT} = 0.93 \omega_{IT}$.

As expected, the results obtained employing the two-oscillator expression (19) based on the RWA are shifted with respect to the results predicted by the SMCA expression (18). For example, the frequency splitting between the UPB and the LPB resulting from Eq. (19), takes the minimal value $\Delta_{\text{ICP}}^{\text{min}} = 2\Omega_R^{\text{res}}$ at $k_x = k_x^{\text{res}}$. For comparison, employing Eq. (18), which goes beyond the RWA, one finds that the minimum of the above mentioned splitting appears at k_x slightly smaller than k_x^{res} . In the case of metallic type mirrors, the above mentioned

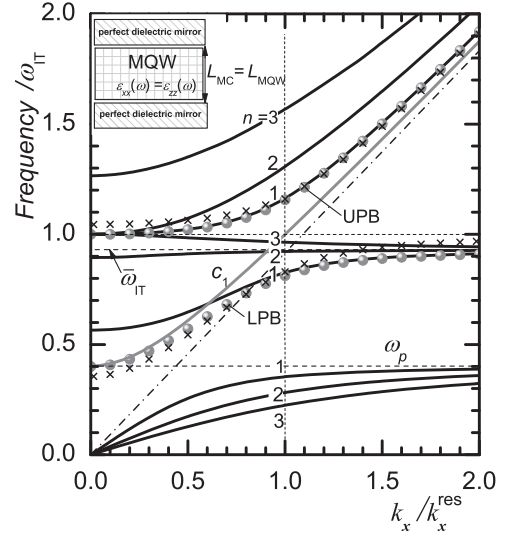


FIG. 1. The normalized frequencies of the three lowest order ($n = 1, 2, 3$) polaritonic branches (solid lines) and the ground photonic mode c_1 (gray solid line) supported by the uniform system with perfect dielectric mirrors ($n_{\min} = 1$), as a function of k_x (see units in text). The geometry of the system is shown in the insert. For illustration, we also present the dispersion of the LPB and the UPB (gray spheres) calculated employing expression (18) which neglects the presence of the intrasubband excitation. The crosses correspond to the LPB and the UPB predicted by the simplified two-oscillator formula (19) based on the RWA. The dot-dashed line corresponds to the light line $\omega = k_x c / \epsilon_w^{1/2}$. The modes at the extreme right-hand side of the diagram between $\omega = 0$ and $\omega = \omega_p$ are essentially the intrasubband Coulomb modes, while the branches laying between $\omega \approx \bar{\omega}_{IT}$ and $\omega = \omega_{IT}$ are basically the intersubband Coulomb modes. The modes located above the light line transform for large wave vector into photonic modes. $\omega_{\perp} = 0.4 \omega_{IT}$, $\omega_p = 0.4 \omega_{IT}$, and $f_{12} = 0.86$. It corresponds to $n^* = 2$, $\theta_{\text{res}} = 68^\circ$, and $\bar{\omega}_{IT} = 0.93 \omega_{IT}$.

frequency splitting takes the minimal value exactly for k_x at which $\varpi_0(k_x) = \bar{\omega}_{IT}$.²⁶

We would like to stress that the eigenvalue equation (17) includes the effects connected with intra- and interwell Coulomb couplings. It is well known that in the case of QWs with parabolic confining potential the static and dynamic intrawell coupling can be omitted.^{8,10} The influence of the above mentioned fact on the behavior of the LPB and UPB supported by model I is considered in Appendix D.

Moreover, when the two lowest subbands are occupied, the two (normal) intersubband plasmon modes become optically active (see, e.g., Ref. 52). In this limit, the semiclassical approach (see Appendix A) in agreement with the microscopic quantum electrodynamic approach,²⁷ predicts the appearance of the photon mediated coupling²² between the above mentioned intersubband plasmon modes.

c. Intrasubband cavity polaritons. Now we discuss the case when only intrasubband transitions are present ($\epsilon_{zz} = \epsilon_w$). Since this paper is devoted to the intersubband polaritons the properties of the intrasubband cavity polaritons will be discussed very briefly without illustrative numerical calculations.

The simplification $\epsilon_{zz} = \epsilon_w$ has a very good justification if $\omega_p^2, \omega^2 \ll \omega_{IT}^2$. In this limit, the dispersion equation (13) for

the n th-order ($n > 0$) intrasubband polariton branches reduces to the form

$$(\omega^2 - \omega_p^2)(\omega^2 - \omega_n^2) = \omega_p^2 n^2 \omega_\perp^2. \quad (20)$$

Solving the above equation one gets the frequencies of the lower ($-, n$) and upper ($+, n$) type intrasubband polariton branches:

$$(\omega_{\pm, n}^{\text{intra}})^2 = \frac{\omega_p^2 + \omega_n^2}{2} \pm \sqrt{\frac{(\omega_p^2 - \omega_n^2)^2}{4} + \omega_p^2 n^2 \omega_\perp^2}. \quad (21)$$

The upper (lower) type branches are located above (below) the plasma frequency ω_p . The n th upper branch starts at $[\omega = (\omega_p^2 + n^2 \omega_\perp^2)^{1/2}, k_x = 0]$ and approaches the n th cavity mode at large k_x . The lower type branches start at $(\omega = 0, k_x = 0)$ and approach ω_p at large k_x .

When $(\omega_p/2\omega_\perp)^2 \ll 1$, the coupling between cavity modes and intrasubband plasmon is strongly nonresonant. Making appropriate expansions in Eq. (21) one finds that the upper type branches practically coincide with the photonic modes while the lower type branches are well modeled by the intrasubband Coulomb modes described by Eq. (15). The situation changes when inequality $\omega_\perp/2 < \omega_p$ is fulfilled. In this case, the coupling between the lowest cavity mode c_1 and the lowest intrasubband Coulomb mode C_1^{intra} takes a resonant character. As expected, in the above mentioned regime, the anticrossing of the polariton branches is predicted by Eq. (21). This equation also predicts formation of the polariton gap. The gap is bounded by the frequencies ω_p and $(\omega_p^2 + \omega_\perp^2)^{1/2}$. It means that in the presently considered limit the system exhibits the USC regime.

d. Hybrid intersubband-intrasubband cavity polaritons. The simultaneous coupling of the cavity mode with the intersubband and intrasubband excitations can be equivalently considered as photon mediated coupling between the intersubband and intrasubband plasmonic modes.²² The above mentioned coupling can lead to the violation of the SMCA through the creation of the ICP branches with an admixture of the intrasubband plasmon. It is reasonable to expect that practically only the low-frequency part of the LPB should be affected by the admixture of the C_1^{intra} mode. The numerical results displayed in Fig. 1 are consistent with the above prediction. As it was mentioned, this figure presents the dispersion characteristics of the polaritonic modes supported by model I with dielectric mirrors. The gray spheres corresponds to the ‘‘pure’’ LPB and UPB described by Eq. (18). The solid curve, with index $n = 1$, located between $\omega = \omega_p$ and $\omega = \bar{\omega}_{\text{IT}}$ (above $\omega = \bar{\omega}_{\text{IT}}$), can be considered as a hybrid LPB (UPB). It is clear that in the large wave vector region ($k_x > k_x^{\text{res}}$) the admixture of the intrasubband plasmon to ICP branches is small. Consequently, their blue shift, with respect to the pure branches is negligibly small. For example, at $k_x = k_x^{\text{res}}$, the blue shift of the LPB takes the value close to $0.014 \omega_{\text{IT}}$. As expected, the blue shift of the LPB increases with the decrease of k_x . At $k_x \cong 0.6 k_x^{\text{res}}$ and $\omega \cong 0.7 \omega_{\text{IT}}$, the hybrid LPB branch crosses photonic mode c_1 and transforms into the upper intrasubband polariton branch [see Eq. (21)] when $k_x \rightarrow 0$. The blue shift of the hybrid LPB at the crossing point is already substantial ($\cong 0.056 \omega_{\text{IT}}$).

As it was mentioned, the UPB, in contrast with the LPB, is practically unaffected by the intrasubband transition. The solid curve corresponding to the hybrid UPB coincides with the curve corresponding to the pure UPB. Consequently, the minimal frequency separation between the hybrid ICP branches is also, but very weakly, affected by the intrasubband excitation. The simulations show that the modifications of the ICP characteristics associated with the presence of the intrasubband excitation are more strongly pronounced on the ω - φ plane than on the ω - k_x plane (see Appendix E).

2. Model II

Now we discuss the properties of the ICP supported by the strongly nonuniform model II. We focus on the role of the radiative coupling (between cavity modes), which is directly associated with the light reflection by the Q2DEG. For simplicity, we neglect the presence of the intrasubband excitation and assume that the system is symmetric.

Let us assume for a moment that the mirrors are of a dielectric type. Then, from Eq. (11), one finds that the characteristic equation can be written as

$$0 = (t_{\text{QW}} + r_{\text{QW}})e^{i\beta_{\text{MC}}} + 1, \quad (22)$$

$$0 = (t_{\text{QW}} - r_{\text{QW}})e^{i\beta_{\text{MC}}} - 1. \quad (23)$$

The modes take symmetric [the normal component of the electric field $E_z(z)$ is even function] and antisymmetric [$E_z(z)$ is odd function] forms. Substituting relation (C10) into Eq. (23) we get the solutions corresponding to pure asymmetric cavity modes ($c_{n=2,4,6,\dots}$). It means that the above modes do not interact with the intersubband plasmon supported by the centrally positioned QW. The solutions of Eq. (22) describe polariton branches resulting from the coupling of the intersubband plasmon with symmetric cavity modes ($c_{n=1,3,5,\dots}$). Taking into account Eqs. (C9) and (C10), we can rewrite Eq. (22) as

$$\frac{\hat{\Lambda}}{2} = \frac{\exp(i\beta_{\text{MC}}) + 1}{\exp(i\beta_{\text{MC}}) - 1} \equiv -i \cot(\beta_{\text{MC}}/2). \quad (24)$$

The explicit expressions for $\beta_{\text{MC}} = k_{w,z} L_{\text{MC}}$ and $\hat{\Lambda} = (4\pi/c\sqrt{\varepsilon_w})\sigma_{zz}k_x^2/K_w k_{w,z}$ are given in Appendix C. Substituting the above mentioned expressions into Eq. (24) and taking $c \rightarrow \infty$, we find that the frequency of the intersubband Coulomb mode (\hat{C}^{inter}) supported by system QW-MC with dielectric type mirrors can be written as

$$\omega_{\hat{C}^{\text{inter}}} = \sqrt{\omega_{\text{IT}}^2 - \omega_p^2 \hat{F} \mathcal{W} / \coth \mathcal{W}}, \quad (25)$$

where $\mathcal{W} = k_x L_{\text{MC}}/2$ and $\hat{F} = f_{12} L_{\text{QW}}^{\text{eff}}/L_{\text{MC}}$.

One can check that in the case of the perfect metallic mirrors $\coth \mathcal{W}$, appearing in Eq. (25), should be replaced by $\tanh \mathcal{W}$. Thus the frequency $\omega_{\hat{C}^{\text{inter}}}$ of the intersubband Coulomb mode supported by model II is smaller than ω_{IT} . The above mentioned fact can be associated with the presence of the image part of the Coulomb interaction.^{51,53} As already mentioned, in the approach based on the dipolar gauge this interaction is mediated by an exchange of cavity photons. Note that the difference between ω_{IT} and $\omega_{\hat{C}^{\text{inter}}}$ increases nearly linearly with increasing k_x (see Fig. 2). The explanation of this

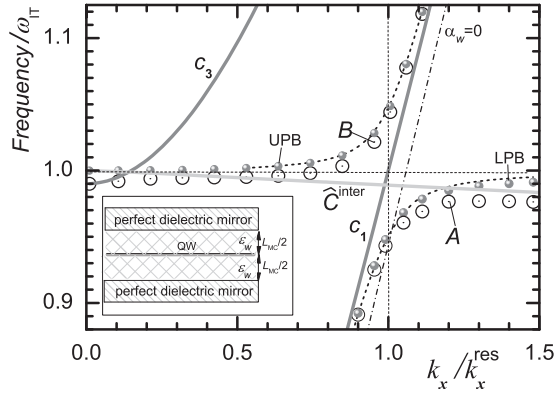


FIG. 2. The normalized frequencies of the photonic modes c_1 and c_3 (gray solid curves) and the two lowest polaritonic branches A and B supported by the QW-MC system with dielectric mirrors (model II) as a function of k_x (see units in text). The circles are obtained employing the “exact” Eqs. (31) and (32), which take into account the higher ($n > 1$) photonic modes. The gray spheres correspond to the results obtained employing Eq. (30) in which the contribution of the higher photonic modes is neglected. The short dashed curves are obtained employing the simplified oscillator model based on the RWA. The light gray solid curve corresponds to the frequency of the intersubband Coulomb mode as given by Eq. (25). The dot-dashed line represents the light line $\alpha_w = 0$. The geometry of the system is shown in the insert. $\omega_{\perp} = 0.33 \omega_{IT}$ and $\hat{F}^{-1/2} \omega_P = 0.07 \omega_{IT}$. It corresponds to $\hat{\Omega}_R^{\text{res}} = 0.047 \omega_{IT}$, $\theta_{\text{res}} = 72.5^\circ$, and $n^* = 3$.

unphysical behavior of $\omega_{\hat{c}_{\text{inter}}}$ will be presented at the end of this section.

Initially, we concentrate on the nearly resonant case ($k_x \approx k_x^{\text{res}}$). We expand the right-hand side of Eq. (24) around $\omega = \omega_1(k_x)$ and make simplifications consistent with the RWA (see Ref. 22). Performing appropriate manipulations one finds that the dispersion equation corresponding to the LPB and UPB reduces, like in the case of uniform model I, to the form predicted by the two-oscillator model ($\omega - \omega_{IT})(\omega - \omega_1) = \hat{\Omega}_R^{\text{res}}$. The resonant Rabi frequency (corresponding to the QW-MC system) is defined by $\hat{\Omega}_R^{\text{res}} = (2\hat{F})^{1/2} (\omega_P/2) \sin \theta_{\text{res}}$. Note that the factors \hat{F} and F [see Eq. (16)] are connected by the relation $F/\hat{F} = L_{MC}/d_{MQW} = N_{QW}$. It implies that the resonant Rabi frequency $\hat{\Omega}_R^{\text{res}}$ corresponding to the uniform MQW-MC system transforms to the above mentioned Rabi frequency $\hat{\Omega}_R^{\text{res}}$ after the replacement $N_{QW} \rightarrow N_{QW}^{\text{eff}} = 2$. Thus $N_{QW}^{\text{eff}} = 2$ can be treated as an effective number of QWs in the presently considered configuration. It is obvious that the value of the Rabi frequency (and consequently N_{QW}^{eff}) generally depends on the type of the mirrors and on the location of the QW inside the MC.⁴⁷

On the other hand, employing the multibeam interference analysis (see Appendix D in Ref. 5) we get quite a different result. Namely, one finds that $N_{QW}^{\text{eff}} = 1$ for the arbitrary type of the mirrors and arbitrary position of the QW inside the MC. Moreover, the antisymmetric photonic modes become optically active. The above mentioned difference can be attributed to the fact that the multibeam interference analysis completely neglects light reflection by the Q2DEG. More precisely, it neglects an (destructive/constructive) interference between the

signal directly reflected by the mirrors and the signal re-emitted from the Q2DEG.⁵⁴

Now, going beyond the RWA, we show that the characteristic equation (11) corresponding to model II can be rewritten in the form showing explicitly the influence of the higher photonic modes on the behavior of the polariton branches. Let us divide the ω - k_x plane into the regions located within and outside the light cone (of the spacer material). The edge of the light cone is defined by the light line $\alpha_w \equiv -ik_{w,z} = 0$ (or, equivalently, $\omega = k_x c/\varepsilon_w^{1/2}$). Within (outside) the light cone, the quantity $\beta_{MC} = k_{w,z} L_{MC}$ [see Eq. (C15)] is real (imaginary). Performing appropriate manipulations and taking into account relations (F1) and (F2) we can rewrite the dispersion equation (11) as

$$\omega^2 - \omega_{IT}^2 = \sum_n \frac{4\omega_{IT}\varpi_n \hat{\Omega}_{R,n}^2}{\omega^2 - \varpi_n^2}, \quad (26)$$

with

$$\hat{\Omega}_{R,n} = \frac{\omega_P}{2} \left(\hat{F} \mathcal{D}_n \frac{\varpi_n}{\omega_{IT}} \right)^{1/2} \sin \theta_n, \quad (27)$$

where $\mathcal{D}_n = \delta_{n,0} + 2\delta_{n,l=2,4,6\dots}$ ($\mathcal{D}_n = 2\delta_{n,l=1,3,5\dots}$) in the case of perfect metallic (dielectric) mirrors.

The above equation has the same form as the eigenvalue equation corresponding to a system composed of harmonic oscillator, with the frequency ω_{IT} , linearly coupled to n ($\rightarrow \infty$) independent oscillators associated with photonic modes c_n .⁵⁰ Consequently, the quantity $\hat{\Omega}_{R,n}$ can be considered as a (dipolar gauge) coupling frequency between the intersubband plasmon supported by the QW and the n th cavity mode.

As already noted, in the SMCA only the coupling of the ground photonic mode with intersubband excitation is considered. It means that the above mentioned approximation corresponds to retaining in Eq. (26) only the term $n = n_{\text{min}}$.

Below, restricting to the SMCA, we will extend the dispersion (26) to the case of a system containing an arbitrary number of the QWs positioned at $z_{N=1,2,3\dots N_{QW}}$. Analogously to our previous paper⁵ (see also Ref. 26), we define the generalized overlap coefficient

$$\begin{aligned} \mathcal{O}_{nn_{\text{min}}} &= \sum_{N=1}^{N_{QW}} \mathcal{E}_n(z_N) \mathcal{E}_{n_{\text{min}}}(z_N) \\ &\cong N_{QW} \int_{MQW} \mathcal{E}_n(z) \mathcal{E}_{n_{\text{min}}}(z) dz, \end{aligned} \quad (28)$$

where $\mathcal{E}_n(z)$ is the normalized mode function describing the spatial variation of the normal component of the electric field (E_z) associated with the n th cavity mode. Writing Eq. (29), we have assumed that the MQW slab contains a large number of the QWs ($N_{QW} \gg 1$).

Retaining in Eq. (26) only the lowest-order term $n = n_{\text{min}}$ and replacing $\mathcal{D}_{n_{\text{min}}}$ by $\mathcal{O}_{n_{\text{min}}n_{\text{min}}}$, we get

$$(\omega^2 - \omega_{IT}^2)(\omega^2 - \varpi_{n_{\text{min}}}^2) = 4\omega_{IT}\varpi_{n_{\text{min}}} \hat{\Omega}_R^2, \quad (30)$$

where $\hat{\Omega}_R$ is defined by Eq. (27) with $\mathcal{D}_{n_{\text{min}}}$ replaced by $\mathcal{O}_{n_{\text{min}}n_{\text{min}}}$. The quantity $\mathcal{O}_{n_{\text{min}}n_{\text{min}}}$ can be treated as an effective number of the QWs interacting with the ground cavity mode. In the case of the uniform system the product $\hat{F} \mathcal{O}_{n_{\text{min}}n_{\text{min}}}$ reduces to factor F and we recover the result predicted by model I.

Equation (30) is consistent with the quantum-mechanical results (based on the SMCA) reported by Todorov and Sirtori.²⁶

The inspection of Eqs. (26)–(29) (see also Refs. 47 and 5) suggests that the coupling of the intersubband excitation with the higher photonic modes starts to play a nonnegligible role when (i) the system exhibits the SSC regime and (ii) the nondiagonal overlap coefficients $\mathcal{O}_{(n>n_{\min})n_{\min}}$ become comparable with the diagonal coefficient $\mathcal{O}_{n_{\min}n_{\min}}$.

Now we discuss the influence of the above mentioned coupling on the behavior of the LPB and the UPB supported by model II. Let us assume that the mirrors are of a dielectric type ($\mathcal{D}_n = 2\delta_{n,l=1,3,5,\dots}$). Within the light cone (where $\beta_{\text{MC}} = k_{w,z}L_{\text{MC}}$ is real), Eq. (24) can be written in the form containing explicitly the mode index

$$n = \left(\frac{\omega^2 - \omega_{\parallel}^2}{\omega_{\perp}^2} \right)^{1/2} - \frac{2}{\pi} \arctan \left[\frac{\pi}{2} \frac{\omega_{\parallel}^2}{\omega_{\perp}(\omega^2 - \omega_{\parallel}^2)^{1/2}} \frac{\widehat{F}\omega_P^2}{\omega^2 - \omega_{\text{IT}}^2} \right]. \quad (31)$$

The branches predicted by the above equation will be labeled A, B, C, \dots in the order of increasing β_{MC} . In the absence of the coupling between intersubband excitation and photonic modes ($\widehat{F}\omega_P^2 \rightarrow 0$) the above mentioned branches transform into photonic modes.

Outside the light cone (where β_{MC} is imaginary), Eq. (24) can be written as

$$-\frac{\pi}{2} \frac{\omega_{\parallel}^2}{\omega_{\perp}(\omega_{\parallel}^2 - \omega^2)^{1/2}} \frac{\widehat{F}\omega_P^2}{\omega^2 - \omega_{\text{IT}}^2} = \coth \left[\frac{\pi(\omega_{\parallel}^2 - \omega^2)^{1/2}}{2\omega_{\perp}} \right]. \quad (32)$$

The above equation, in contrast with Eq. (31), has only one solution. This solution can be treated as the continuation of branch A originating within the light cone.

We discuss numerically and analytically the behavior of branches A and B taking $\widehat{F}^{1/2}\omega_P = 0.07\omega_{\text{IT}}$ and $\omega_{\perp} = 0.33\omega_{\text{IT}}$. It corresponds to $\widehat{\Omega}_R^{\text{res}} = 0.047\omega_{\text{IT}}$, $\theta_{\text{res}} = 72.5^\circ$, $n^* = 3$, and $\varpi_3(k_x^{\text{res}}) = 1.37\omega_{\text{IT}}$. Open circles in Fig. 2 display the k_x dependence of the branches A and B obtained employing the “exact” expressions (31) and (32). (The higher branches are not presented since they practically coincide with the higher photonic modes.) To illustrate the restricted validity of the RWA and the SMCA, in Fig. 2, we also display the behavior of the UPB and the LPB predicted by (i) the simplified two-oscillator model (based on the RWA) and (ii) the SMCA expression (30), which includes the non-RWA terms but neglects the coupling with higher photonic modes.

Note that in the presently considered system the normalized Rabi splitting $2\widehat{\Omega}_R^{\text{res}}/\omega_{\text{IT}}$ is rather small ($\cong 0.1$). It explains why the frequencies of the LPB and the UPB predicted by the oscillator model (see short dashed lines in Fig. 2), practically coincide with the frequencies predicted by Eq. (30) based on the SMCA (see gray spheres in Fig. 2). However, the results displayed in Fig. 2 show that despite the small value of the ratio $2\widehat{\Omega}_R^{\text{res}}/\omega_{\text{IT}}$, the corrections resulting from the coupling with higher cavity modes cannot be treated as negligibly small. As expected, the above mentioned coupling affects

branches A and B (represented by circles in Fig. 2) in a slightly different way.

First, we discuss the behavior of branch B . We find from Fig. 2 that this branch starts at $\varpi_3(k_x = 0) = 0.99\omega_{\text{IT}}$, crosses the line $\omega = \omega_{\text{IT}}$ at $k_x^{\text{cr}} \cong 0.75k_x^{\text{res}}$ and approaches monotonically ϖ_1 at large k_x . Note that at ω close to ω_{IT} the (imaginary) parameter $\widehat{\Lambda}$, appearing in Eq. (24), takes very large values. Thus the expansion $\arctan x = (\pi/2)(x/|x|) - 1/x$ (valid for $|x| \gg 1$) can be used in Eq. (31). Employing this expansion, one finds that branch B changes, with increasing k_x , its mode index (from $n = 3$ to 1) during the crossing of the line $\omega = \omega_{\text{IT}}$. The above mentioned transformation is associated with the simultaneous coupling of the intersubband plasmon with the ground (c_1) and higher ($c_{n=3,5,7,\dots}$) photonic modes. At $k_x \cong k_x^{\text{cr}}$, where branch B changes its mode index, c_1 and c_3 cavity modes are nearly symmetrically positioned with respect to ω_{IT} . It is obvious that the admixture of higher photonic modes (mainly c_3) is responsible for the redshift of branch B with respect to the pure UPB predicted by the SMCA expression (30). Results displayed in Fig. 2 show that the above mentioned shift is substantial only for $k_x \lesssim k_x^{\text{res}}$.

Now we discuss the influence of the coupling with higher photonic modes on the behavior of branch A represented by circles in Fig. 2. As one can expect, the above mentioned coupling also leads to the redshift of branch A with respect to the pure LPB predicted by the SMCA and represented by circles in Fig. 2. Now, however, this redshift becomes substantial when $k_x \gtrsim k_x^{\text{res}}$. The inspection of Fig. 2 shows that the asymptotic behavior of branch A is quite different than the asymptotic behavior of the pure LPB. Namely, branch A is not monotonic with k_x . In the presently discussed system, it reaches the maximum value ($\approx 0.978\omega_{\text{IT}}$) at $k_x \cong 1.3k_x^{\text{res}}$ and then decreases very slowly with increasing k_x . At large values of k_x its behavior is well modeled by the dispersion of the intersubband Coulomb mode $\widehat{C}^{\text{inter}}$ given by Eq. (25). For comparison, the pure LPB approaches asymptotically the frequency $\widehat{\omega}_{\text{IT}} = (\omega_{\text{IT}}^2 - 2\omega_P^2\widehat{F})^{1/2} \approx 0.995\omega_{\text{IT}}$.

As already mentioned, the phenomena described above can be interpreted as a result of the coupling intersubband excitation with the higher photonic modes. Simulations show that at $k_x = 1.5k_x^{\text{res}}$, the contribution of $n = 3$ and $n > 3$ cavity modes to the redshift experienced by the A branch is close to 34% and 66%, respectively. Note that the role of the above mentioned modes increases with increasing k_x . One can check that at sufficiently large $k_x \gg \hat{k}_{x,n}$ ($\hat{k}_{x,n}$ is determined by relation $\omega_{\parallel}(k_x) = n\omega_{\perp}$) the contribution of the n th cavity mode, to the right-hand side of Eq. (26), very weakly depends on its mode index. This fact can be associated with the formation of the negative slope of branch A at $k_x \gtrsim 1.3k_x^{\text{res}}$. However, we should remember that the dispersion equations (31) and (32) are based on the sheet model. Unfortunately, the violation of this model or, more precisely, the violation of the LWA is expected when the index of the photonic mode n (interacting with the intersubband excitation) is sufficiently large ($\gtrsim L_{\text{MC}}/L_{\text{QW}}^{\text{eff}}$). In this limit, the variation of E_z (connected with photonic modes) in the region occupied by the Q2DEG cannot be treated as negligibly small. Consequently, the coupling strength with higher photonic modes is substantial overestimated by the sheet model.

We should also remember that the role of the higher photonic modes decreases dramatically when we replace a single QW by an MQW slab with a thickness L_{MQW} comparable with the cavity width L_{MC} . Employing the concept of the generalized overlap coefficient (29), one can check that the influence of higher photonic modes on the behavior of the LPB and UPB decreases very fast with increasing photonic mode index.⁵ For illustration, let us assume that the MQW (with the thickness $L_{\text{MQW}} = L_{\text{MC}}/2$) is located asymmetrically in the space between perfect dielectric mirrors. In such systems, the ground cavity mode couples radiatively with the asymmetric cavity modes ($n = 2, 4, 6, \dots$). The normalized nondiagonal overlap coefficients $\mathcal{O}_{1n}/\mathcal{O}_{11}$, associated with this coupling, take, for $n = 2, 4$ and 6 , the values $0.85, 0.34$, and 0.22 , respectively. It supports (see also Fig. 8) the statement that the role of the higher photonic modes (or equivalently, their admixture to the LPB and UPB) decreases with increasing the MQW thickness.

Also note that in the case of the realistic systems the effective modal volume increases with the increasing mode index (see, e.g., Fig. 1 in Ref. 14). It should lead to an additional reduction of the coupling strength with higher photonic modes.

The polariton dispersion curves, with a qualitatively similar behavior to that presented in Fig. 2, have been predicted for excitonic polaritons, supported by a multimode dielectric waveguide with embedded QW, employing the semiclassical⁵⁵ and quantum-mechanical⁵⁶ approaches. Moreover, the asymptotic behavior of branch A is qualitatively similar to the behavior of the lowest polariton branch supported by the planar waveguide with perfectly conducting walls when one of the walls is covered by a thin layer of a “nondissipative” metal.⁵⁷

B. Systems with plasmonic mirrors

So far, we have studied the properties of the polariton modes assuming that the mirrors are perfect and the ohmic dissipation is negligibly small. In this section we briefly discuss the main consequences of the above mentioned simplifications. We pay special attention to the systems with plasmonic mirror(s) [see, e.g., Fig. 3(b)]. An important feature of the above mentioned mirrors is the strong ω dependence (dispersion) of their characteristics (see Fig. 4). It complicates the solution of the dispersion equation (7) even when its simplified version (8) is employed. Nevertheless, in the case of nearly resonant systems exhibiting the ordinary strong coupling regime, useful analytical expressions can also be obtained making appropriate simplifications. We restrict ourselves to the discussion of φ -dependent characteristics of virtual modes. As it was mentioned, such characteristics are directly measured. The k_x -dependent dispersion can be extracted numerically from the φ -dependent characteristics employing relation (2). Such type of calculations are performed in Sec. IV for systems displayed in Fig. 3.

Let us assume that the MQW slab, backed by the spacer layers with dielectric constant $\varepsilon_{s1} = \varepsilon_w$, is located between the mirrors characterized by the ω -dependent reflection coefficients r_l ($l = b, c$). As already mentioned, we concentrate on systems exhibiting the ordinary strong coupling regime. It means that a simplified Eq. (8), omitting the radiative coupling

effects (connected with light reflection by the Q2DEG), can be employed.

It is convenient for further discussion to define the mirror phase shift in the following way:

$$r_l(\omega) = -\varrho_l(\omega)e^{i\Phi_l(\omega)}, \quad (33)$$

where $\varrho_l = \sqrt{R_l}$ and Φ_l (R_l) is the phase shift (the energy reflection coefficient) of the l th mirror. In the case of perfect dielectric mirrors $\Phi_l = 0$ and $R_l = 1$. Below, we discuss realistic systems where $\Phi_l \neq 0$ and $R_l < 1$.

Taking into account the definition (33), we can transform Eq. (8) into the following form:

$$k_{\text{MQW},z}L_{\text{MC}} = \pi(n - \Phi_{\text{mirr}}/2\pi) + i\varrho_{\text{mirr}}/2, \quad (34)$$

where $\Phi_{\text{mirr}} = \Phi_b + \Phi_c$ is the total mirror phase shift, $\varrho_{\text{mirr}} = \ln \varrho_b \varrho_c$ and n is mode index.

In further discussion we neglect for simplicity the intrasubband excitation (generalization is straightforward). Expanding $k_{\text{MQW},z}$ in a power series³⁸ and employing the relation $k_{w,z} = K_w \cos \varphi$ one can rewrite Eq. (34) into a more convenient form:

$$\omega = \underline{\omega}_1 \left[\left(n - \frac{\Phi_{\text{mirr}} - \Lambda''}{2\pi} \right) + i \frac{\varrho_{\text{mirr}} - \Lambda'}{2\pi} \right], \quad (35)$$

where $\underline{\omega}_1 = \omega_{\perp}/\cos \varphi$ is the φ -dependent frequency of the ground photonic mode of the MC with perfect dielectric mirrors (see Appendix E) and $\Lambda \equiv \Lambda' + i\Lambda'' = N_{\text{QW}}(4\pi/c\sqrt{\varepsilon_w})\sigma_{zz} \tan \varphi \sin \varphi$.

Then we assume that ω is close to the resonant angle φ_{res} defined by the relation $\omega_{\text{IT}} = \omega'_1(\varphi)$, where $\tilde{\omega}_1(\varphi) = \omega'_1(\varphi) + i\omega''_1(\varphi)$ is the complex frequency of the ground photonic mode of the considered MC. As it was noted, when the mirrors are of a plasmonic type, the quantities Φ_{mirr} and ϱ_{mirr} , appearing in Eq. (35), depend strongly on ω . With no loss of generality they can be written in the form

$$\Phi_{\text{mirr}}(\omega) = \Phi_{\text{mirr}}^{\text{res}} + (\omega - \omega_{\text{IT}})\Phi' + \Phi_{\text{nl}}(\omega), \quad (36)$$

$$\varrho_{\text{mirr}}(\omega) = \varrho_{\text{mirr}}^{\text{res}} + (\omega - \omega_{\text{IT}})\varrho' + \varrho_{\text{nl}}(\omega), \quad (37)$$

such that $\Phi_{\text{nl}}(\omega)$ and $\varrho_{\text{nl}}(\omega)$ contain only second- and higher-order variations with ω , and such that $\Phi_{\text{nl}}(\omega_{\text{IT}}) = \varrho_{\text{nl}}(\omega_{\text{IT}}) = 0$. For convenience, we have introduced the notation $\Phi_{\text{mirr}}^{\text{res}} = \Phi_{\text{mirr}}(\omega_{\text{IT}})$ and $\varrho_{\text{mirr}}^{\text{res}} = \varrho_{\text{mirr}}(\omega_{\text{IT}})$.

It is obvious that in the case of a nearly resonant system ($\varphi \approx \varphi_{\text{res}}$) exhibiting the ordinary strong coupling regime, only the narrow frequency range, around ω_{IT} , can be considered. (We assume that in the above mentioned frequency range quantities Φ_{mirr} and Φ' are positive.) In the first approximation, we can take into account only the linear dependence of $\Phi_{\text{mirr}}(\omega)$ and $\varrho_{\text{mirr}}(\omega)$ on ω (the linear limit). It is equivalent to the assumption $\Phi_{\text{nl}}(\omega) = \varrho_{\text{nl}}(\omega) = 0$. Let us neglect for a moment (i) the intersubband excitation and (ii) the ω -dependence of $\varrho_{\text{mirr}}(\omega)$ assuming that $\varrho_{\text{mirr}}(\omega) = \varrho_{\text{mirr}}^{\text{res}}$. Then, from Eqs. (35)–(37), one finds that the complex frequency of the ground cavity mode can be approximated by

$$\tilde{\omega}_1 = \underline{\omega}_1 \left[\left(1 - \frac{\Phi_{\text{mirr}}^{\text{res}} - \omega_{\text{IT}}\Phi'}{2\pi} \right) + i \frac{\varrho_{\text{mirr}}^{\text{res}}}{2\pi} \right] \frac{L_{\text{MC}}}{L_{\text{MC}}^{\text{eff}}}, \quad (38)$$

where $L_{\text{MC}}^{\text{eff}} = L_{\text{MC}}(1 + \Phi'\underline{\omega}_1/2\pi)$ is an effective thickness of the MC. The above equation is consistent with the expression

derived by Panzarini *et al.*⁵⁸ for the MC with the distributed Bragg reflectors (DBRs).

The inspection of Eq. (38) leads to an important conclusion that the linear dispersion of Φ_{mirr} implies the reduction of the cavity mode broadening by factor $L_{\text{MC}}/L_{\text{MC}}^{\text{eff}}$ compared to the nondispersive case $\Phi_{\text{mirr}} = \Phi_{\text{mirr}}^{\text{res}}$. The ω dependence of ϱ_{mirr} practically does not affect the above conclusion. One can check that the effects connected with the linear dependence of ϱ_{mirr} on ω are controlled by the parameter $\mathcal{R} = \underline{\omega}_1 \varrho' L_{\text{MC}} / 2\pi \varrho_{\text{mirr}}^{\text{res}} L_{\text{MC}}^{\text{eff}}$. As long as the ground cavity mode can be treated as a well-defined entity (i.e., when $\omega_1'(\varphi_{\text{res}}) \gg |\omega_1''(\varphi_{\text{res}})|$), the above mentioned parameter is small. It means that the photonic mode is very weakly affected by the ϱ_{mirr} dispersion. The situation is more complex in the case of the polariton branches, i.e., when the intersubband excitation is included.

Employing Eqs. (35)–(38) and (A4) and performing appropriate manipulations, one finds that the angle-resolved spectra of the LPB and the UPB are determined by the following equation:

$$(\omega - \tilde{\omega}_1)(\omega - \tilde{\omega}_{\text{IT}}) = \Omega_{\text{res}}^2 L_{\text{MC}} / L_{\text{MC}}^{\text{eff}} (1 - i\mathcal{R}), \quad (39)$$

where $\Omega_{\text{res}}^2 = F(\omega_p/2)^2 \tan^2 \varphi_{\text{res}}$, $\tilde{\omega}_{\text{IT}} = \omega_{\text{IT}} - i\gamma_{\text{IT}}$ and γ_{IT} is the intersubband dephasing rate. The inspection of Eqs. (38) and (39) leads to the following conclusions. As long as only the linear dispersion of the mirror phase shift Φ_{mirr} is present, the angle-resolved spectra of the nearly resonant structure can be modeled by the two-coupled oscillator formula. It describes two oscillators having complex frequencies $\tilde{\omega}_{\text{IT}}$ and $\tilde{\omega}_1$. The coupling between them is determined by the effective (resonant) coupling frequency $\Omega_{\text{res}}(L_{\text{MC}}/L_{\text{MC}}^{\text{eff}})^{1/2}$. It means that the linear dispersion of the phase shift not only reduces the cavity mode broadening but also decreases the effective coupling frequency with respect to the constant phase shift case ($\Phi_{\text{mirr}} = \Phi_{\text{mirr}}^{\text{res}}$). In the case of the perfect mirrors the difference between L_{MC} and $L_{\text{MC}}^{\text{eff}}$ vanishes and the above mentioned coupling is quantified by frequency Ω_{res} (see Appendix E).

We would like to emphasize fact that the discussed above effective coupling frequency determines the minimal separation between constant-angle (virtual) polariton branches ($\Delta_{\text{ICP}}^{\text{min}}$). This quantity practically coincides with the polariton peak splitting in the angle-resolved spectra. As mentioned in Introduction (see also the next section), $\Delta_{\text{ICP}}^{\text{min}}$ is substantially larger than the minimal polariton branch splitting $\Delta_{\text{ICP}}^{\text{min}}$ on the ω - k_x plane.

The ω dependence of ϱ_{mirr} leads to the additional renormalization of the effective coupling frequency. Equation (39) indicates that the linear dispersion of ϱ_{mirr} can be included replacing the real effective coupling frequency $\Omega_{\text{res}}(L_{\text{MC}}/L_{\text{MC}}^{\text{eff}})^{1/2}$ by the complex quantity $\Omega_{\text{res}}[L_{\text{MC}}/L_{\text{MC}}^{\text{eff}}(1 - i\mathcal{R})]^{1/2}$. It implies, in agreement with the experimental results reported in Refs. 12 and 11, the asymmetry of the linewidth behavior at the anticrossing for the LPB and the UPB. Thus the polariton branch broadening is not well reproduced by the two-coupled oscillator formula when ϱ_{mirr} depends on ω .

Deriving Eq. (39), we have neglected the nonlinear term in the mirror phase shift dispersion (36). This term leads to additional modifications of the cavity and polariton spectra. First of all, it shifts the photonic mode frequencies. The above

mentioned shift depends, in general, on the cavity mode index n . It means that the presence of higher order terms in the phase shift dispersion prevents the perfect uniformity of the cavity mode spacing on the ω - φ plane. The above conclusion is consistent with numerical simulations based on the TMF (see Ref. 5). One can also check that the presence of the nonlinear term can lead to the enhancement of the minimal polariton peak splitting $\Delta_{\text{ICP}}^{\text{min}}$. In other words, the nonlinear term partially compensates for the reduction of $\Delta_{\text{ICP}}^{\text{min}}$ induced by the linear phase shift dispersion.

Discussing the consequences of the replacement of perfect dielectric mirrors by plasmonic mirrors, we have assumed that the mirror phase shift Φ_{mirr} , appearing in the dispersion equation (35) is positive ($\Phi_{\text{mirr}} > 0$). However, at a sufficiently low frequency ($\omega < \omega_{p,\text{mirr}}$), the above mentioned quantity can be negative [see, e.g., Fig. 4(e)]. It means that in the case of the systems with plasmonic mirrors the formation of a new type of the radiative type cavity eigenmodes—surface plasmon polariton modes is potentially possible (see Appendix G). The consequences of this fact are discussed in the next section.

IV. NUMERICAL RESULTS AND DISCUSSION

A. Description of samples and mirror characteristics

Numerical calculations reported in this section are performed for three structures called: \mathcal{A} , \mathcal{B} , and \mathcal{C} . They are schematically presented in Fig. 3. We assume, for simplicity, that in all the considered structures the QWs will be treated as two-subband systems. Additionally, performing the numerical calculations, we assume for simplicity that the intersubband

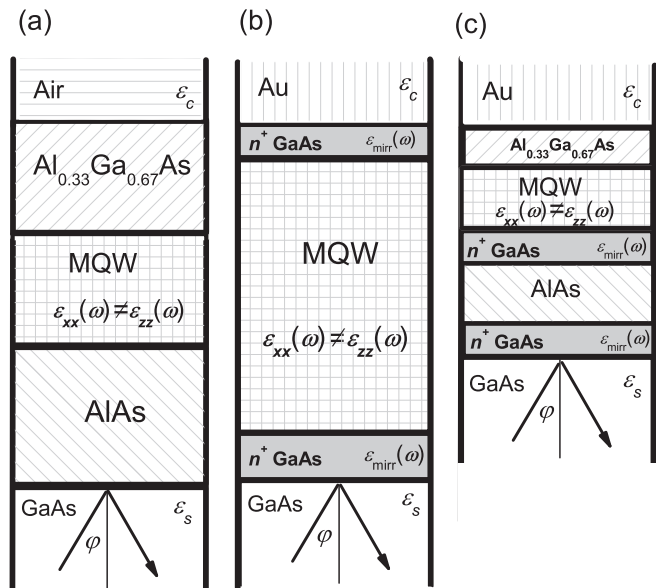


FIG. 3. Diagrams illustrating schematically the geometry of the three structures discussed in the paper: (a) structure \mathcal{A} , (b) structure \mathcal{B} , and (c) structure \mathcal{C} . The regions occupied by the n -doped dielectric layers (or multilayers) playing the role of the plasmonic mirrors are shaded. The above mentioned layers are described by Drude-like dielectric function $\varepsilon_{\text{mirr}}(\omega)$ given in Appendix G.

dephasing rate (γ_{T}) coincides with the intrasubband dephasing rate (γ_{\parallel}).

The first structure (\mathcal{A}), with purely dielectric mirrors, is similar to that studied recently in Refs. 12 and 11. It is grown on a GaAs substrate ($\epsilon_s = \epsilon_{\text{GaAs}}$) and consists of a MQW (with $N_{\text{QW}} = 50$) embedded between undoped AlAs layer (coupling mirror) and undoped $\text{Al}_{0.33}\text{Ga}_{0.67}\text{As}$ spacer layer with thicknesses of $2.5 \mu\text{m}$ and $2 \mu\text{m}$, respectively. The cladding medium is air ($\epsilon_c = 1$). The period of the MQW consists of a 90-\AA GaAs QW and a 300-\AA $\text{Al}_{0.33}\text{Ga}_{0.67}\text{As}$ barrier. We also take the surface electron density $N_s = 2 \times 10^{12} \text{ cm}^{-2}$ (corresponding to the plasma frequency $\omega_p = 31.5 \text{ meV}/\hbar$), $\hbar\omega_{\text{T}} = 120 \text{ meV}$, $f_{12} = 0.86$ and $2\hbar\gamma_{\text{T}} = 7.5 \text{ meV}$.

Structure \mathcal{B} is similar to that studied experimentally by Dupont *et al.*^{2,14} and theoretically in our previous paper.⁵ It is also grown on a GaAs semi-insulating substrate and consists of a MQW (with $N_{\text{QW}} = 140$) embedded between a $0.4\text{-}\mu\text{m}$ -thick n^+ GaAs top layer and $0.8\text{-}\mu\text{m}$ -thick n^+ GaAs bottom layer (coupling mirror) with the doping concentration $N_D = 2 \times 10^{18} \text{ cm}^{-3}$. The above mentioned doping corresponds to the plasma frequency of the mirror material $\omega_{p,\text{mirr}} = 62 \text{ meV}/\hbar$. The cladding medium is Au. The period of the MQW consists of a 60-\AA GaAs QW and a 290-\AA $\text{Al}_{0.21}\text{Ga}_{0.79}\text{As}$ barrier. The QW is described by the following parameters: $\hbar\omega_{\text{T}} = 114 \text{ meV}$, $f_{12} = 0.86$, $2\hbar\gamma_{\text{T}} = 6.2 \text{ meV}$, and $N_s = 2 \times 10^{11} \text{ cm}^{-2}$ ($\hbar\omega_p = 10.5 \text{ meV}$).

Structure \mathcal{C} corresponds to the system studied by Anappara *et al.*⁶ It is grown on the GaAs substrate. The coupling mirror is realized by sandwiching a $1.65\text{-}\mu\text{m}$ -AlAs layer between two GaAs layers doped to $5 \times 10^{18} \text{ cm}^{-3}$ ($\hbar\omega_{p,\text{mirr}} = 98 \text{ meV}$), each having a thickness of 1500 \AA . The active region consists of 70 repeats of n -doped 65-\AA -thick GaAs QWs separated by 80-\AA -thick $\text{Al}_{0.35}\text{Ga}_{0.65}\text{As}$ barriers. A 1000-\AA -thick $\text{Al}_{0.35}\text{Ga}_{0.65}\text{As}$ spacer layer is located between the MQW and a cladding medium (Au). We also take $\hbar\omega_{\text{T}} = 152 \text{ meV}$, $2\hbar\gamma_{\text{T}} = 12 \text{ meV}$, $f_{12} = 0.86$, and $N_s = 3.25 \times 10^{12} \text{ cm}^{-2}$ ($\hbar\omega_p = 66 \text{ meV}$).

Figure 4 displays the ω dependence of the power reflection coefficient $R_{b(c)}$ and the mirror phase shift $\Phi_{b(c)}$ corresponding to the resonant configuration ($\varphi = \varphi_{\text{res}}$). In the case of structures \mathcal{B} and \mathcal{C} , we additionally present mirror characteristics obtained assuming that the mirror material dielectric function $\epsilon_{\text{mirr}}(\omega) \equiv \epsilon_{n^+\text{GaAs}}(\omega)$ (see Appendix G) does not depend on ω . More precisely, we assume that $\epsilon_{\text{mirr}}(\omega) = \epsilon_{\text{mirr}}(\omega_{\text{T}})$. For convenience, we also assume that in structures \mathcal{A} , \mathcal{B} , and \mathcal{C} , the back mirror corresponds to $2\text{-}\mu\text{m}$ -thick $\text{Ga}_{0.33}\text{Al}_{0.67}\text{As}$ spacer layer bounded by air, the $0.4\text{-}\mu\text{m}$ -thick n^+ GaAs layer bounded by Au, and the 1000-\AA -thick $\text{Ga}_{0.33}\text{Al}_{0.67}\text{As}$ spacer layer bounded by Au, respectively.

The results displayed in Fig. 4 indicate that in structure \mathcal{A} only R_c and Φ_b manifest strong ω dependence. However, we should remember that the nearly linear variation of the back mirror phase shift Φ_b with ω is mainly connected with the presence of the $\text{Ga}_{0.33}\text{Al}_{0.67}\text{As}$ spacer layer. Simulations show that in the absence of this layer, Φ_b is nearly independent on ω .

A much more interesting situation occurs in the case of plasmonic mirrors. Figure 4 very well illustrates the fact that the ω dependence of ϵ_{mirr} leads to the substantial dispersion of the mirror characteristics. Note that the above mentioned

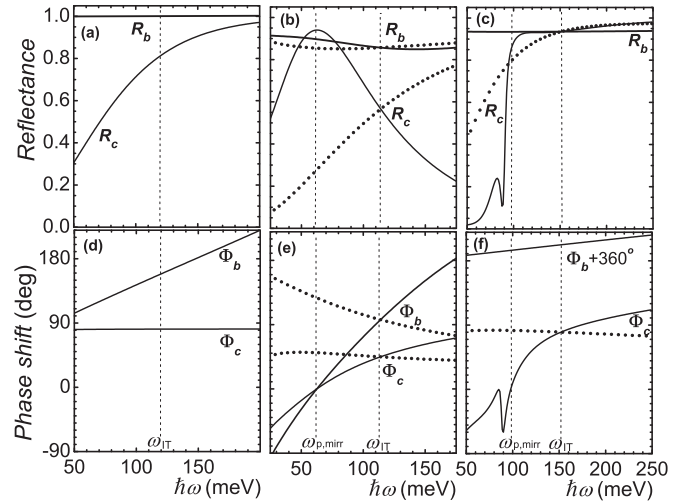


FIG. 4. The spectral dependence of the mirror reflectivities R_b and R_c (upper panels) and the phase shifts Φ_b and Φ_c (lower panels) calculated for the resonant structures \mathcal{A} (the left panels), \mathcal{B} (the central panels) and \mathcal{C} (the right panels). The solid (dotted) curves are obtained taking into account [neglecting; $\epsilon_{\text{mirr}}(\omega) = \epsilon_{\text{mirr}}(\omega_{\text{T}})$] of the mirror material dispersion. For convenience of the presentation, the curve displaying the ω dependence of Φ_b in structure \mathcal{C} has been shifted by 360° .

dispersion is, in general, nonlinear. In the case of single layer mirrors (like in structure \mathcal{B}) the nonlinearity is not very strong. Nevertheless, it substantially disturbs the perfect uniformity of the cavity mode spacing on the ω - φ plane [see Fig. 2(a) in Ref. 5]. Figure 4 also supports our previous statement that in the case of the plasmonic mirror the phase shift becomes negative at the frequency smaller than mirror plasma frequency $\omega_{p,\text{mirr}}$. As expected the omission of the mirror material dispersion [more precisely replacement $\epsilon_{\text{mirr}}(\omega)$ by $\epsilon_{\text{mirr}}(\omega_{\text{T}})$] leads to a drastic reduction of the mirror phase shift dispersion.

It is seen from Fig. 4 that the behavior of the multilayer plasmonic mirror, employed in structure \mathcal{C} , is more complex compared to the single layer case. For example, we observe the appearance of the dip (at $\hbar\omega \approx 90 \text{ meV}$) in the ω dependence of R_c and Φ_c . Since in the system discussed here the mirror plasma frequency $\omega_{p,\text{mirr}}$ is close to $98 \text{ meV}/\hbar$, the appearance of the dip can be associated with the formation of the (radiative) surface plasmon polariton mode (see Appendix H). At this point we would also like to stress that a slightly similar situation takes place in the case of DBRs. However, in the above mentioned system the formation of so-called leaky modes (below and above the stop band at $k_x \approx 0$) is responsible for the appearance of additional structures in the spectra of reflection coefficient.^{23,24} It is obvious that the formation of the leaky modes in the DBRs is not connected with surface plasmon polaritons but with the interference of the wave in periodic dielectric structures.⁵⁸

B. Polariton dispersion characteristics

1. The φ -dependent characteristics

Let us first consider the φ -dependent characteristics. As already mentioned, such characteristics can be

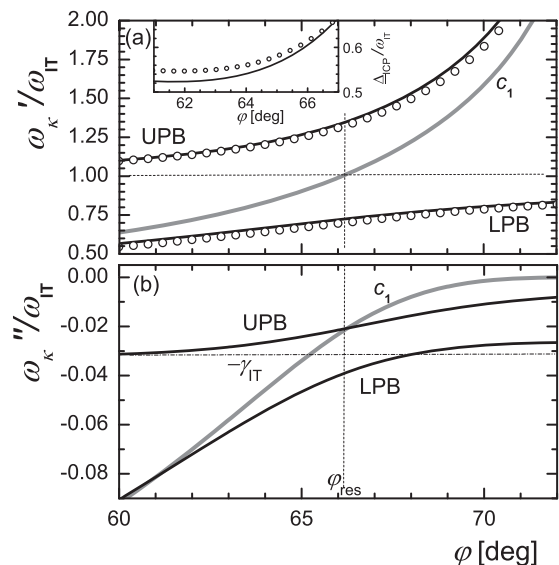


FIG. 5. The real part (upper panel) and the imaginary part (lower panel) of the normalized frequencies of the modes c_1 , UPB and LPB supported by structure \mathcal{A} as a function of φ . The insert shows the φ dependence of the polariton branch separation Δ_{ICP} . For illustration, we additionally present the results obtained including only resonant term in expression for σ_{zz} (open circles in the upper panel).

directly determined by angle-resolved reflectance-absorbance measurements.

The complex frequencies ($\tilde{\omega}_\kappa = \omega'_\kappa + i\omega''_\kappa$) of constant-angle virtual modes have been calculated numerically employing the TMF supplemented by the “microscopic” EMA. For clarity only the lowest-order virtual modes are discussed. The behavior of higher-order modes ($n > 1$) supported by the structures with dielectric and plasmonic mirrors has been partially discussed in our previous papers.^{4,5}

The numerical results corresponding to structure \mathcal{A} are displayed in Fig. 5. They are consistent with the predictions resulting from the simplified model discussed in Sec. III B. For example, in agreement with the experimental results reported in Refs. 12 and 11, we find that due to strong ω dependence of R_c the anticrossing of curves corresponding to the real part of the polariton frequencies (ω'_{LPB} and ω'_{UPB}) is not accompanied by the crossing of curves corresponding to the imaginary part of the polariton frequencies (ω''_{LPB} and ω''_{UPB}). Note also that in the considered structure, the UPB is narrower than the ground photonic mode and the intersubband resonance ($|\omega'_{UPB}| < \gamma_{IT}, |\omega''_{c_1}|$) for $60^\circ \lesssim \varphi \lesssim 66^\circ$, while for $62^\circ \lesssim \varphi \lesssim 68^\circ$ the linewidth of the LPB exceeds the linewidth of both photonic mode and the intersubband resonance ($|\omega'_{LPB}| > \gamma_{IT}, |\omega''_{c_1}|$). The insert in Fig. 5 shows the variation of the polariton branch separation $\Delta_{ICP} = \omega'_{UPB} - \omega'_{LPB}$ (on the ω - φ plane). Examining this insert, one finds that the minimal branch separation appears not at $\varphi \approx \varphi_{res} \cong 66.1^\circ$, as the simplified two-coupled oscillator expression (39) suggests, but at $\varphi \cong 62^\circ$. We suppose that this fact can be associated with radiative coupling effects (see below).

Results presented in the upper panel of Fig. 5 also illustrates the statement that neglecting the nonresonant term in the

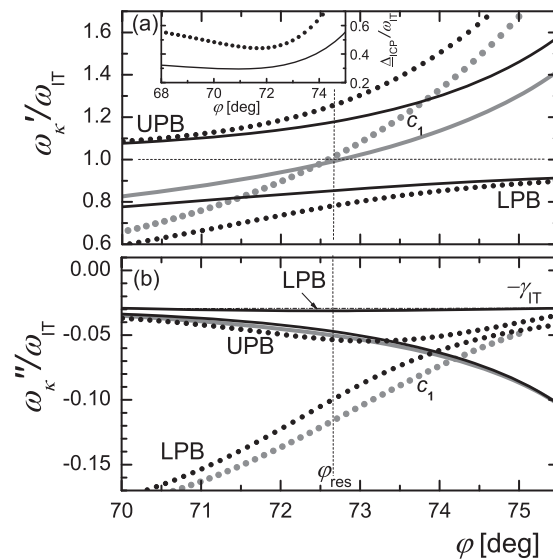


FIG. 6. The real part (upper panel) and the imaginary part (lower panel) of the normalized frequencies of the modes c_1 , UPB and LPB supported by structure \mathcal{B} as a function of φ . The solid (dotted) curves are obtained taking into account [neglecting; $\varepsilon_{mirr}(\omega) = \varepsilon_{mirr}(\omega_{IT})$] the mirror material dispersion. In the lower panel the solid curves corresponding to the modes c_1 and UPB practically cannot be distinguished. Moreover, the difference between ω''_{LPB} and $-\gamma_{IT}$ is also negligibly small. The insert shows φ dependence of the polariton branch separation Δ_{ICP} .

expression for σ_{zz} (see Appendix A) leads to a very small redshift of the polariton branches. As expected, this shift rather weakly affects the minimal branch separation. Numerical simulations (results are not presented) suggest that the above remarks are also valid for structures \mathcal{B} and \mathcal{C} .

Figure 6 displays the behavior of the constant-angle virtual modes supported by structure \mathcal{B} with plasmonic mirrors. Calculations have been performed taking into account (solid curves) as well as neglecting (dotted curves) the dispersion of the mirror material, i.e., taking $\varepsilon_{mirr}(\omega) = \varepsilon_{mirr}(\omega_{IT})$. For clarity, we do not present the behavior of the (radiative) A_{SP} surface plasmon polariton mode supported by the passive MC (see Appendix G). As one can expect the above mode is located slightly below the surface plasmon frequency $\omega_{p,mirr}^{surf} = \omega_{p,mirr}/\sqrt{2} (\cong 0.38 \omega_{IT})$. The complex frequency of the above mentioned plasmonic type mode rather weakly depends on φ and can be approximated by $\tilde{\omega}_{ASP}(\varphi_{res}) \cong 0.36 \omega_{IT} + i0.018 \omega_{IT}$ where $\varphi_{res} \cong 72.6^\circ$. It is obvious that the presently considered plasmonic type mode does not appear when $\varepsilon_{mirr}(\omega)$ is replaced by $\varepsilon_{mirr}(\omega_{IT})$.

The above mentioned replacement leads, in agreement with analytical results presented in Sec. III B, to the substantial modification of the polariton branch dispersion. From the insert in Fig. 6 one finds that, in the presence of the mirror dispersion, the polariton branch separation Δ_{ICP} (in structure \mathcal{B}) takes the minimal value of $0.3 \omega_{IT}$ at $\varphi \cong 70.9^\circ$. When the mirror dispersion is neglected, i.e., when $\varepsilon_{mirr}(\omega) = \varepsilon_{mirr}(\omega_{IT})$ the above mentioned separation takes the minimal value of $0.44 \omega_{IT}$ at $\varphi \cong 71.7^\circ$. It is interesting to note that the above

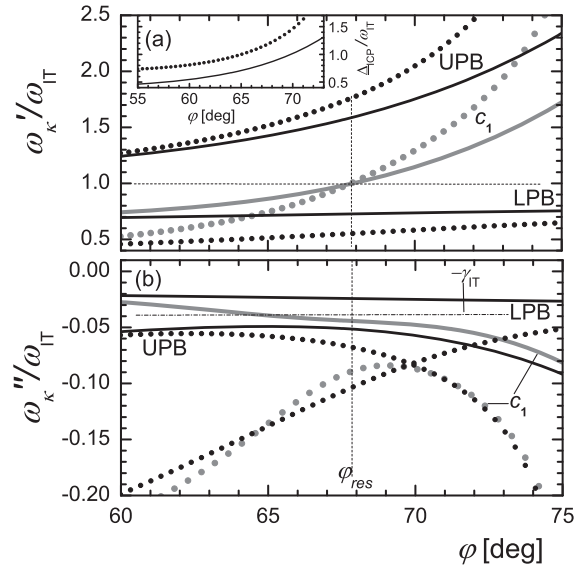


FIG. 7. The real part (upper panel) and the imaginary part (lower panel) of the normalized frequencies of the modes c_1 , UPB, and LPB supported by structure \mathcal{C} as a function of φ . The solid (dotted) curves are obtained taking into account [neglecting; $\varepsilon_{\text{mirr}}(\omega) = \varepsilon_{\text{mirr}}(\omega_{\text{IT}})$] the mirror material dispersion. The insert shows the φ dependence of the polariton branch separation Δ_{ICP} .

mentioned replacement affects rather weakly the polariton dispersion on the ω - k_x plane (see Fig. 9).

Figure 6(b) also shows that due to strong ω dependence of R_c , we do not observe the crossing of the curves ω''_{LPB} and ω''_{UPB} at φ close to φ_{res} . Since R_c decreases with increasing ω , the linewidth of the LPB is smaller than the UPB. The above finding is in qualitative agreement with the experimental results reported by Dupont *et al.*^{2,14}

The angular dispersion of the virtual modes supported by structure \mathcal{C} is displayed in Fig. 7. The resonant angle φ_{res} is close to 67.9° . Like in the case of structure \mathcal{B} we do not present the behavior of the surface plasmon polariton mode supported by the passive MC. The real part of the frequency of this mode varies between $0.5 \omega_{\text{IT}}$ and $0.7 \omega_{\text{IT}}$.

The inspection of the Figs. 6 and 7 shows that the behaviors of the UPB and the LPB in structures \mathcal{B} and \mathcal{C} do not differ dramatically. Nevertheless, some differences are noticeable. For example, due to a larger value of the normalized Rabi splitting in structure \mathcal{C} , compared to structure \mathcal{B} [see Figs. 9 and 10], the branch separation Δ_{ICP} in the former system decreases with decreasing φ .

2. The k_x -dependent characteristics

The k_x -dependent characteristics for the virtual modes supported by structures \mathcal{A} , \mathcal{B} , and \mathcal{C} have been extracted from φ -dependent characteristics (see Figs. 5–7) employing relation (2). The results of the calculations are displayed in Figs. 8–10. To facilitate the comparison with results predicted by model I and model II the frequency is plotted as a function of the dimensional quantity k_x/k_x^{res} . k_x^{res} corresponds to the in-plane wave vector at which the first order cavity mode is in the resonance with the intersubband transition or

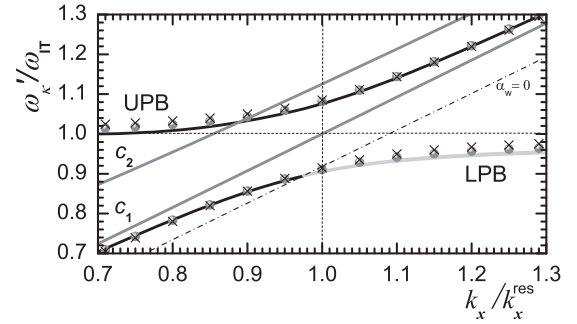


FIG. 8. The real part of the normalized frequencies of the modes c_1 , c_2 , UPB, and LPB supported by structure \mathcal{A} as a function of k_x (see units in text). The gray solid curve, starting at $k_x \cong 0.97 k_x^{\text{res}}$, corresponds to part of the LPB having a nonradiative character. The gray spheres represent results obtained employing the SMCA (see text). The crosses represent results obtained with the help of Eq. (19) corresponding to the simplified oscillator model. The dot-dashed line represents the substrate light line.

more precisely when $\omega'_{c_1}(k_x) = \omega_{\text{IT}}$. Simulations show that in structures (\mathcal{A} , \mathcal{B} , \mathcal{C}) k_x^{res} is close to $(1.83, 1.82, \text{ and } 2.35 \mu\text{m}^{-1})$.

We should remember that only the constant-angle virtual modes corresponding to photonic modes and the UPBs have a radiative character for arbitrary k_x , i.e., they are located within the substrate light cone. The constant-angle virtual mode representing the LPB crosses, at $\varphi = 90^\circ$, the substrate light line and transforms continuously into the nonradiative type mode.⁴⁵ It means that only part of the (k_x -dependent) dispersion curve of the LPB (which is located within the substrate light cone) can be extracted employing the above mentioned approach.

From results presented in Figs. 8–10 one finds that, in structures (\mathcal{A} , \mathcal{B} , \mathcal{C}) the LPB crosses the substrate light line at $k_x = k_x^{\text{max}}$ close to $(0.97 k_x^{\text{res}}, 1.01 k_x^{\text{res}}, 0.83 k_x^{\text{res}})$. It is obvious that the dispersion of the LPB for $k_x > k_x^{\text{max}}$ (where the above branch has a nonradiative character) can be also obtained solving numerically a characteristic equation (1). Then, however, we have to assume that the in-plane wave vector k_x is a real quantity. The mode frequency has to be

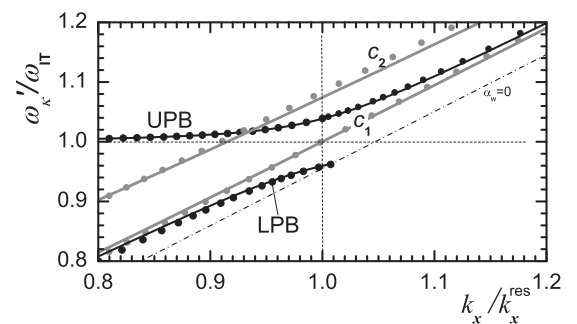


FIG. 9. The real part of the normalized frequencies of the modes c_1 , c_2 , UPB and LPB supported by structure \mathcal{B} as a function of k_x (see units in text). Results are obtained including (solid curves) and neglecting (dotted curves) of the mirror material dispersion. The dot-dashed line represents the substrate light line.

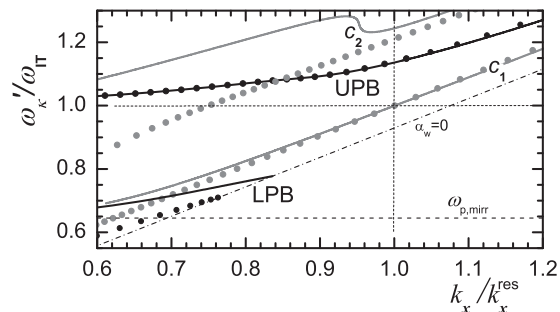


FIG. 10. The real part of the frequencies of the modes c_1 , c_2 , UPB, and LPB supported by structure \mathcal{C} as a function of k_x (see units in text). Results are obtained both including (solid curves) and neglecting (dotted curves) the mirror material dispersion. The dot-dashed line represents the substrate light line.

considered as a complex quantity as long as the nonradiative losses are present.^{45,46}

Our simulations show that the minimal values of the normalized polariton branch splitting $\Delta_{\text{ICP}}^{\text{min}}/\omega_{\text{IT}}$ (on the ω - k_x plane) achieve values close to (0.17, 0.08, 0.3) in structures (\mathcal{A} , \mathcal{B} , \mathcal{C}). Thus it is reasonable to expect that the considered systems should exhibit the SSC. To illustrate the correctness of the above mentioned statement we additionally display the dispersion characteristics of the second order photonic modes (see curves in Figs. 8–10 denoted as c_2). The obtained results fully confirm the above mentioned suggestion. For structures (\mathcal{A} , \mathcal{B} , \mathcal{C}), the ratio $\Delta_{\text{ICP}}^{\text{min}}/\Delta_{\text{CM}}$ takes values close to (1.3, 1.1, 1.3).

As demonstrated in Sec. III A, in the (nonuniform) systems exhibiting the SSC, the coupling with higher photonic modes cannot be excluded *a priori*. Below, we show evidence indicating that such a situation takes place in the case of structure \mathcal{A} . We concentrate only on structure \mathcal{A} because modes supported by structures \mathcal{B} and \mathcal{C} can be substantially affected by plasmonic effects.

To facilitate a qualitative comparison with results predicted by model II, we have additionally calculated [solving numerically Eq. (1)] the dispersion characteristic of the LPB in the region where the above branch has a nonradiative character, i.e., for $k_x > k_x^{\text{max}}$. Moreover, simultaneously with the exact numerical results (solid black and gray curves), the results obtained with the help of the SMCA expression (30) (gray spheres) and the simplified oscillator model (crosses) are presented for structure \mathcal{A} in Fig. 8. In the two latter cases, the product $\widehat{F}\mathcal{O}_{11}\omega_p^2$ [appearing in Eq. (30)] was treated as a fitting parameter. The k_x -dependence of the ground photonic mode frequency was extracted from the TMF results. It is clear that the deviation of the exact results from those predicted by the SMCA expression (30) has the same qualitative character as that observed in the QW-MC system studied in Fig. 2. It is interesting to note that similar type deviations [see the behavior of the UPB in Fig. 4(b) in Ref. 5] are also observed in the case of structure \mathcal{B} but when only half of the space between the mirrors is occupied by QWs. The above findings support our statement that in realistic systems exhibiting the SSC regime the effects associated with radiative mode coupling cannot be neglected *a priori*.

In the case of structures \mathcal{B} and \mathcal{C} , the effects connected with the formation of surface-plasmon modes should be additionally considered. We concentrate on structure \mathcal{C} because only in this structure the difference between intersubband transition frequency ω_{IT} and mirror plasma frequency $\omega_{p,\text{mirr}}$ (or more precisely surface plasmon frequency $\omega_{p,\text{mirr}}^{\text{surf}} = \omega_{p,\text{mirr}}/\sqrt{2}$) is comparable with Rabi splitting $\Delta_{\text{ICP}}^{\text{min}}$. From Fig. 10, we find that the low frequency part of the LPB is blueshifted with respect to the nondispersive case $\varepsilon_{\text{mirr}}(\omega) = \varepsilon_{\text{mirr}}(\omega_{\text{IT}})$. The low-frequency part of mode c_1 experiences also the blue shift but it is substantially smaller than the blue shift of the LPB. We suppose that the above mentioned fact is mainly associated with the radiative coupling of mode c_1 with the surface plasmonic mode(s). However, some contribution of the effects connected with the (photon mediated) coupling between the intersubband and intrasubband plasmons cannot be excluded. Nevertheless, the relative role of this coupling should be rather small due to its a strongly nonresonant character. (The origin of the peculiar behavior of the c_2 mode observed, in Fig. 10, at $k_x \lesssim 0.95 k_x^{\text{res}}$ will be discussed in future publications.)

It is reasonable to expect that the consequence of the coupling between the inter- and intrasubband plasmons can be enhanced drastically introducing the modification to the MQW system, similar to that discussed by Plumridge *et al.*³⁶ The period of the modified structure should contain, except a typical QW, an additional heavily n -doped semiconductor layer(s). The insertion of the above mentioned “metallic” layer(s) increases the plasma frequency, associated with the electron motion in the x - y plane, but does not substantially affect the intersubband resonant frequency.

Discussing the role of the surface plasmonic modes we have concentrated on the systems where the above mentioned modes are not resonant with intersubband plasmon. However, the system can be also designed so as to achieve the resonant coupling between the surface plasmonic modes and intersubband excitation. Preliminary simulations, performed for structure \mathcal{B} with ω_{IT} treated as a free parameter, predict the formation of the multiple peak structure in absorption spectra when ω_{IT} approaches $\omega_{p,\text{mirr}}^{\text{surf}}$. The above mentioned multiple peak structure can be associated with the formation of the intersubband surface plasmon polariton branches. The results reported in Ref. 31 suggest that they can have interesting new properties (dispersion characteristics) controlled by the ratio $\omega_{p,\text{mirr}}^{\text{surf}}/\omega_{\perp}$. We are planning to discuss this problem in a separate paper.

As it was mentioned in Introduction, planar systems are considered in this paper. Nevertheless, it is worth noting that the USC between the intersubband excitation and photonic modes supported by zero-dimensional (0D) metallic MCs is also observed.^{7–9,27} In the above mentioned systems, subwavelength confinement (in the z direction) takes place. Some remarks connected with this fact are presented below.

It is obvious that in the case of the planar system with subwavelength thickness only the fundamental $c_0 \equiv \text{TM}_0$ mode (with E_z that is constant through the MC) can be considered. The (periodical) lateral patterning of the above mentioned system leads to the formation of 0D metallic MCs with a lateral photonic confinement due to the impedance mismatch between the double and single metal regions. It can be assumed that in the lateral direction the structure simply

behaves like a set of independent Fabry-Perot resonators. Changing the length and/or width of the stripes one can obtain the resonance conditions between the intersubband excitation and lateral photonic modes (TM_{*m*n0}) of the 0D metallic MC.^{7-9,27} It is reasonable to expect that the lateral patterning also affects the intersubband Coulomb modes. However, different quantization conditions can be expected for the radiation and material excitations. Note that in the case of 0D metallic MCs the lateral photonic mode separation becomes comparable with Rabi frequency when the system enters into the USC regime. It means that in the above mentioned situation not only the multi-normal-mode splitting is potentially possible but also the formation of the polariton branches with an admixture of many lateral photonic modes should not be excluded *a priori*. A more detailed discussion of the above mentioned problem is beyond the scope of this paper.

V. CONCLUSIONS

The properties of the ICP modes in realistic MQW-MC systems have been investigated theoretically employing a semiclassical approach based on the TMF supplemented by the “microscopic” EMA and the sheet model. Numerical calculations have been completed by the analytical calculations performed for simplified models.

Simulations reveal that the correct interpretation of the ICP spectra supported by the strongly nonuniform structure, with pure dielectric or plasmonic mirrors, should go beyond the commonly used SMCA when systems enter into the SSC regime. In this regime, the Rabi splitting becomes comparable to/larger than the separation between cavity modes and more than one cavity modes can, in principle, interact with intersubband excitation. Consequently, a formation of the LPB and the UPB having a non-negligible admixture of higher photonic modes and/or surface plasmonic modes becomes possible.

Moreover, we have shown that the polariton dispersion characteristics predicted by the semiclassical approach are consistent with those resulting from a recently developed microscopic quantum approach^{26,27} provided that we work in the SMCA. Demonstrating the above mentioned consistency, we have also presented the evidence indicating that in the MQW-MC systems exhibiting the USC the interwell Coulomb coupling plays an important role.

ACKNOWLEDGMENT

The authors thank Y. Todorov and M. Geiser for discussions.

APPENDIX A: EFFECTIVE DIELECTRIC TENSOR AND COULOMB MODES

The “microscopic” implementation of the EMA leads to the following expression for the components of the diagonal effective dielectric tensor $\epsilon(\omega)$:³⁸

$$\epsilon_{\alpha\alpha}(\omega) = (1 - f_{\text{QW}})\epsilon_b + f_{\text{QW}}\epsilon_w + \Sigma_{\alpha}(\omega), \quad \alpha = x, y, \quad (\text{A1})$$

$$\epsilon_{zz}^{-1}(\omega) = (1 - f_{\text{QW}})/\epsilon_b + f_{\text{QW}}/\epsilon_w - \Sigma_z(\omega)/\epsilon_w^2, \quad (\text{A2})$$

where $f_{\text{QW}} = L_{\text{QW}}/d_{\text{MQW}}$, L_{QW} is the thickness of the QW, d_{MQW} is the period of the MQW, and $\Sigma_{\rho}(\omega) = i4\pi\sigma_{\rho\rho}(\omega)/\omega L_{\text{MQW}}$ ($\rho = x, y, z$). $\sigma_{\alpha\alpha}(\omega)$ is an intrasubband (sheet) conductivity of the Q2DEG. It can be taken in the form

$$\sigma_{\alpha\alpha}(\omega) = \frac{N_s e^2}{m^*} \frac{i}{\omega + i\gamma_{\parallel}}, \quad (\text{A3})$$

where γ_{\parallel} is the intrasubband dephasing rate, N_s is the sheet electron density, and m^* is the electron effective mass.

The intersubband sheet conductivity $\sigma_{zz}(\omega)$ describes the nonretarded collective intersubband response of the Q2DEG (embedded in a medium with dielectric constant ϵ_w) to the uniform external electric field $\mathbf{E}^{\text{ext}}(t) = \mathbf{e}_z E_z^{\text{ext}} e^{-i\omega t}$. The self-consistent density functional theory^{53,59} (see also next Appendix) leads to the following expression for $\sigma_{zz}(\omega)$:

$$\sigma_{zz}(\omega) = \frac{N_s e^2 f_{21}}{m^*} \frac{i\omega}{\omega^2 - \omega_{\text{IT}}^2 + i2\omega\gamma_{\text{IT}}}, \quad (\text{A4})$$

where γ_{IT} is the intersubband dephasing rate and f_{12} is the oscillator strength. As it was mentioned, the QW is treated as a two subband system with only the ground subband occupied.

The intersubband resonant frequency ω_{IT} corresponds to the frequency of the intersubband Coulomb mode supported by an isolated QW. When ω is close to ω_{IT} , the nonresonant term in Eq. (A4) plays a negligible role and can be omitted. It is equivalent to the replacement $\omega^2 - \omega_{\text{IT}}^2 \rightarrow 2\omega(\omega - \omega_{\text{IT}})$ (resonant approximation).

In the limiting case discussed in Sec. III, i.e., when $\epsilon_w = \epsilon_b$ and $\gamma_{\text{IT}} = \gamma_{\parallel} = 0$, the components of the effective dielectric tensor, resulting from Eqs. (A1)–(A4), reduce to the form

$$\frac{\epsilon_{\alpha\alpha}(\omega)}{\epsilon_w} = \frac{\omega^2 - \omega_p^2}{\omega^2}, \quad (\text{A5})$$

$$\frac{\epsilon_w}{\epsilon_{zz}(\omega)} = \frac{\omega^2 - \bar{\omega}_{\text{IT}}^2}{\omega^2 - \omega_{\text{IT}}^2}, \quad (\text{A6})$$

where $\bar{\omega}_{\text{IT}}^2 = \omega_{\text{IT}}^2 - f_{12}\omega_p^2$.

The frequency $\omega_p = (4\pi N_s e^2 / d_{\text{MQW}} m^* \epsilon_w)^{1/2}$ coincides with the frequency of the intrasubband plasmon propagating along the z axes of the infinite MQW.³³ The form of Eq. (A2) indicates that $\epsilon_{zz}(\omega)$ has a pole at $\omega = \bar{\omega}_{\text{IT}}$. The above mentioned frequency coincides with the frequency of the intersubband plasmon propagating perpendicularly to z axes of the infinite MQW.³³

When L_{QW} and N_s are not too small, then the random phase approximation can be employed. In this limit, we get^{53,59}

$$\omega_{\text{IT}}^2 = \omega_{21}^2 + \omega_p^2, \quad (\text{A7})$$

$$\omega_p^2 = \omega_p^2(d_{\text{MQW}}/L_{\text{QW}}^{\text{eff}}), \quad (\text{A8})$$

where $L_{\text{QW}}^{\text{eff}} = 2m^*\omega_{21}/\hbar I_{22}$ is the effective thickness of the QW normalized by the Coulomb interaction, $I_{22} = \int_{\text{QW}} \xi_{12}^2(z) dz$, $\xi_{12}(z) = \chi_1(z)\partial_z \chi_2(z) - \chi_2(z)\partial_z \chi_1(z)$, and χ_1 (χ_2) is the envelope function of the ground (excited) subband.

We should remember that the expression for intersubband resonant frequency ω_{IT} presented above has been derived

taking into account only the resonant screening effect. More sophisticated calculations should include not only the dynamic Coulomb effect but also the static (Hartree) charge effects, i.e., the N_s dependence of the subband spacing ω_{21} .^{8,27,59} Fortunately, in the case of typical rectangular QWs (with $L_{\text{QW}} \lesssim 100$ Å), the difference between the intersubband transition frequency ω_{IT} and the intersubband spacing of the bare QW $\omega_{21|N_s=0}$ is determined mainly by the depolarization shift. In the case of parabolic QWs, like those studied experimentally by Geiser *et al.*,¹⁰ the depolarization shift is compensated by the static charge effects and $\omega_{\text{IT}} = \omega_{21|N_s=0}$.⁸

When the number of the occupied subbands increases the number of independent (normal) intersubband plasmon modes supported by the QW also increases. For example, an explicit expression for $\varepsilon_{zz}(\omega)$, corresponding to the system with two occupied subbands (where $\chi_1 \rightarrow \chi_2$ and $\chi_2 \rightarrow \chi_3$ transitions are dominant), can be obtained substituting into (A2) the formula for $\sigma_{zz}(\omega)$ derived in our previous paper.⁵² The equivalent result is predicted by the quantum-mechanical approach.²⁷

The properties of the ICPs supported by the MQW-MC and QW-MC systems with many occupied subbands have also been recently studied (see Refs. 8 and 9). The results reported in the above mentioned papers indicate that when the number of occupied subbands is large, practically only one intersubband plasmonic mode is optically active. It means that, then, the intersubband sheet conductivity takes the same form as that corresponding to the two-subband system.

APPENDIX B: THE PARAMAGNETIC AND RWA INTERSUBBAND CONDUCTIVITIES

In the semiclassical approach based on the minimal-coupling Hamiltonian, the intersubband current density can be divided into the paramagnetic (nonlocal) and diamagnetic (local) contributions.^{43,44,53,60} As it was mentioned, in theoretical papers^{40,44} while discussing the properties of the ICP, the authors neglect the diamagnetic current density term (which depends linearly on the vector potential \mathbf{A}). The consequences of the above mentioned simplification are very briefly discussed below. For completeness, the effects connected with the omission of the counter-rotating term are also considered. Ohmic losses and static charge effects are neglected for simplicity.

We start from the LWA expression for the zz component of the nonlocal intersubband conductivity tensor of the Q2DEG.^{44,60} For our purpose, it is convenient to write the above expression as^{44,60}

$$\sigma_{zz}(k_x = 0, \omega | z, z') = b(\omega) \xi_{12}(z) \xi_{12}(z'), \quad (\text{B1})$$

where

$$b(\omega) = \frac{i e^2 \hbar N_s}{m^* \omega_{21}} \left(\frac{1}{\omega - \omega_{21}} + \frac{1}{\omega + \omega_{21}} \right) \frac{\Upsilon(\omega)}{2}. \quad (\text{B2})$$

When the diamagnetic and counter-rotating terms are included then $\Upsilon(\omega) = 1$. One can check that if the diamagnetic term is omitted then $\Upsilon(\omega) \rightarrow \Upsilon_{\text{par}}(\omega) = \omega_{21}^2 / \omega^2$. On the other

hand, employing the RWA, i.e., omitting the counter-rotating term, we get $\Upsilon(\omega) \rightarrow \Upsilon_{\text{RWA}}(\omega) = (\omega + \omega_{21}) / 2\omega$.

The intersubband sheet conductivity $\sigma_{zz}(\omega)$ is connected with the quantities $b(\omega)$ and I_{22} in the following way:⁴⁴

$$\sigma_{zz}(\omega) = \frac{i \omega \varepsilon_w (2m^* \omega_{21} z_{21} / \hbar)^2}{i \omega \varepsilon_w / b(\omega) - 4\pi I_{22}}. \quad (\text{B3})$$

Deriving the above equation we have used relation $\int_{\text{QW}} \xi_{12}(z) dz = 2m^* \omega_{21} z_{21} / \hbar$, where $z_{21} = \int_{\text{QW}} z \chi_1(z) \chi_2(z) dz$.

It follows from Eqs. (B2), (B3), and (A8) that the expression for $\sigma_{zz}(\omega)$ can be rewritten as

$$\sigma_{zz}(\omega) = \frac{\Upsilon(\omega) N_s e^2 f_{21}}{m^*} \frac{i \omega}{\omega^2 - \omega_{21}^2 - \Upsilon(\omega) \omega_P^2}. \quad (\text{B4})$$

The inspection of the above equation indicates that omission of the diamagnetic or/and counter-rotating term can be taken into account making in the exact expression (A4) for $\sigma_{zz}(\omega)$ the following substitution $N_s \rightarrow N_s \Upsilon(\omega)$. Below, we discuss the influence of the above mentioned substitution on the frequency of the intersubband plasmon supported by the QW.

Let us neglect the diamagnetic term [$\Upsilon(\omega) = \omega_{21}^2 / \omega^2$]. Then, one finds, using Eq. (12) and Eqs. (B2)–(B4), that the intersubband plasmon frequency, at which $1/\sigma_{zz}(\omega) \rightarrow 0$, can be determined from the following relation:

$$\omega^2 (\omega^2 - \omega_{21}^2) - \omega_P^2 \omega_{21}^2 = [\omega^2 - (\omega_+^{\text{par}})^2][\omega^2 - (\omega_-^{\text{par}})^2] = 0, \quad (\text{B5})$$

where $(\omega_{\pm}^{\text{par}})^2 = \omega_{21}^2 [1 \pm \sqrt{1 + (2\omega_P / \omega_{21})^2}] / 2$. Thus the frequency $\omega_+^{\text{par}} (\equiv \omega_{\text{IT}}^{\text{par}})$ can be treated as the paramagnetic intersubband plasmon frequency.

The omission of the counter-rotating term leads to the following relation for the intersubband plasmon frequency:

$$2\omega(\omega - \omega_{21}) - \omega_P^2 = (\omega - \omega_+^{\text{RWA}})(\omega - \omega_-^{\text{RWA}}) = 0, \quad (\text{B6})$$

where $\omega_{\pm}^{\text{RWA}} = \omega_{21} [1 \pm \sqrt{1 + 2(\omega_P / \omega_{21})^2}] / 2$. The frequency $\omega_+^{\text{RWA}} (\equiv \omega_{\text{IT}}^{\text{RWA}})$ can be treated as the RWA intersubband plasmon frequency.

Figure 11 displays the ω_P dependence of ω_{IT} (dotted curve), $\omega_{\text{IT}}^{\text{RWA}}$ (dot-dashed curve) and $\omega_{\text{IT}}^{\text{par}}$ (dot-dot-dashed curve). The static charge effects are omitted. The values in this figure clearly show that the omission of the diamagnetic term, as it was done in Ref. 40, leads to the underestimation of the depolarization shift. For example, at $\omega_P = \omega_{21}$, the omission of the above mentioned term reduces the intersubband resonant frequency from the value of $\omega_{\text{IT}} = 1.41 \omega_{21}$ to $\omega_{\text{IT}}^{\text{par}} = 1.27 \omega_{21}$. Neglecting the counter-rotating term also reduces the depolarization shift. However, this reduction is several times smaller than that associated with the diamagnetic term. As expected, as long as $(\omega_P / \omega_{21})^2 \ll 1$, the difference between ω_{IT} , $\omega_{\text{IT}}^{\text{par}}$, and $\omega_{\text{IT}}^{\text{RWA}}$ is negligibly small.

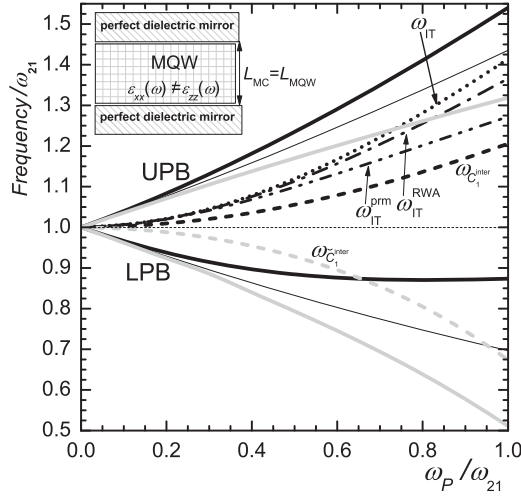


FIG. 11. The frequencies of the ICP branches (solid curves) and the Coulomb modes (dashed curves) supported by the uniform MQW-MC system with perfect dielectric mirrors ($n_{\min} = 1$) as a function ω_p/ω_{21} . Calculations have been performed assuming that the cavity is resonant with the bare intersubband transition $\varpi_1(k_x) = \omega_{21}$. The thick black solid curves and the black dashed curve are obtained employing the “exact” expressions (18) and (14), respectively. The gray solid (dashed) curves are obtained employing Eq. (D3) [Eq. (D4)], in which intrawell coupling is omitted. The thin solid curves are predicted by the one-electron expression (D1) in which the inter- and intrawell Coulomb couplings are omitted. The figure also displays the ω_p dependence of the intersubband resonant frequencies ω_{IT} , ω_{IT}^{prn} , and ω_{IT}^{RWA} predicted by Eqs. (A7), (B5), and (B6), respectively. The static charge effect is neglected. We have used $\omega_{\perp} = 0.3 \omega_{21}$ and $F = 0.6$.

APPENDIX C: CAVITY TRANSFER MATRICES

1. The MQW-MC system

Matrix $\mathbf{I}(r_{l,j})$, accounting for the interface between the media (layers) l and $j (= l + 1)$, is given by³⁸

$$\mathbf{I}(r_{l,j}) = \mathbf{I}^{-1}(r_{j,l}) \equiv \frac{1}{t_{l,j}} \begin{bmatrix} 1 & r_{l,j} \\ r_{l,j} & 1 \end{bmatrix}. \quad (\text{C1})$$

The Fresnel coefficients appearing in the above equation can be written as

$$r_{l,j} = (k_{l,z}\bar{\varepsilon}_j - k_{j,z}\bar{\varepsilon}_l)/(k_{l,z}\bar{\varepsilon}_j + k_{j,z}\bar{\varepsilon}_l), \quad (\text{C2})$$

$$t_{l,j} = 2k_{l,z}\bar{\varepsilon}_j/(k_{l,z}\bar{\varepsilon}_j + k_{j,z}\bar{\varepsilon}_l), \quad (\text{C3})$$

where $\bar{\varepsilon}_{j \neq \text{MQW}} = \varepsilon_j$ and $\bar{\varepsilon}_{j = \text{MQW}} = \varepsilon_{xx}$.

Matrix $\mathbf{L}(\beta_{\text{MQWC}}/2)$ is given by³⁸

$$\mathbf{L}(\beta_{\text{MQWC}}/2) = \begin{bmatrix} e^{-i\beta_{\text{MQWC}}/2} & 0 \\ 0 & e^{i\beta_{\text{MQWC}}/2} \end{bmatrix}. \quad (\text{C4})$$

Substituting Eqs. (C1)–(C4) into (5) and performing appropriate manipulations, we get

$$T_{11}^{\text{cb}} = (e^{-i\beta_{\text{MQWC}}} - r_{\text{MQWC}}^2 e^{i\beta_{\text{MQWC}}}) / (1 - r_{\text{MQWC}}^2), \quad (\text{C5})$$

$$T_{12}^{\text{cb}} = -T_{12}^{\text{cb}} = r_{\text{MQWC}}(e^{-i\beta_{\text{MQWC}}} - e^{i\beta_{\text{MQWC}}}) / (1 - r_{\text{MQWC}}^2), \quad (\text{C6})$$

$$T_{22}^{\text{cb}} = e^{i\beta_{\text{MQWC}}}. \quad (\text{C7})$$

2. The QW-MC system

The transfer matrix corresponding to the sheet can be written as³⁸

$$\mathbf{I}^{2D} = \frac{1}{t_{\text{QW}}} \begin{bmatrix} 1 & -r_{\text{QW}} \\ r_{\text{QW}} & t_{\text{QW}}^2 - r_{\text{QW}}^2 \end{bmatrix}, \quad (\text{C8})$$

with

$$t_{\text{QW}} = 1/(1 + \hat{\Lambda}/2), \quad (\text{C9})$$

$$r_{\text{QW}} = t_{\text{QW}} - 1 = (-\hat{\Lambda}/2)/(1 + \hat{\Lambda}/2), \quad (\text{C10})$$

where $\hat{\Lambda} = (4\pi/c\sqrt{\varepsilon_w})\sigma_{zz}k_x^2/K_w k_{w,z}$.

Employing Eqs. (10), (C4), and (C8), we get

$$T_{11}^{\text{cb}} = \frac{1}{t_{\text{QW}}} e^{-i\beta_{\text{MC}}}, \quad (\text{C11})$$

$$T_{12}^{\text{cb}} = -T_{21}^{\text{cb}} = \frac{-r_{\text{QW}}}{t_{\text{QW}}}, \quad (\text{C12})$$

$$T_{22}^{\text{cb}} = \frac{t_{\text{QW}}^2 - r_{\text{QW}}^2}{t_{\text{QW}}} e^{i\beta_{\text{MC}}}. \quad (\text{C13})$$

In the dissipationless limit, quantities $\hat{\Lambda}$ and β_{MC} are given by

$$\frac{\hat{\Lambda}}{2} = i \frac{\pi^2 \omega_x^2}{4 \omega_{\perp}^2} \frac{\hat{F} \omega_p^2}{\omega^2 - \omega_{\text{IT}}^2} \frac{2}{\beta_{\text{MC}}}, \quad (\text{C14})$$

$$\frac{\beta_{\text{MC}}}{2} = \frac{\pi (\omega^2 - \omega_x^2)^{1/2}}{2 \omega_{\perp}}. \quad (\text{C15})$$

APPENDIX D: THE ROLE OF THE INTERWELL COULOMB COUPLING AND PARABOLIC QWS

In this Appendix, we briefly discuss the role of the intra- and interwell Coulomb couplings in model I neglecting for simplicity the intrasubband excitation. To get the information about the role of the above mentioned couplings it is instructive to consider the eigenvalue equation predicted by the one-electron minimal-coupling Hamiltonian approach developed by Ciuti *et al.*²⁵ The results reported in this paper lead to the eigenvalue equation (for the UPB and the LPB supported by model I) of the following form:

$$(\omega^2 - \omega_{21}^2)(\omega^2 - \hat{\omega}_{n_{\min}}^2) = 4\omega_{21}\varpi_{n_{\min}}\bar{\Omega}_R^2, \quad (\text{D1})$$

where $\hat{\omega}_{n_{\min}}^2 = \varpi_{n_{\min}}^2 + 4\bar{\Omega}_R^2\varpi_{n_{\min}}/\omega_{21}$.

In agreement with Ref. 17 (see also Sec. III D in Ref. 26), we assume that the frequency $\bar{\Omega}_R$ quantifying, in the minimal coupling gauge, the coupling between the ground photonic mode ($c_{n_{\min}}$) and the two electronic conduction subbands, can be taken in the form

$$\bar{\Omega}_R = (f_{12}^{1/2} \omega_p/2)(\omega_{21}/\varpi_{n_{\min}})^{1/2} \sin \theta_{n_{\min}}. \quad (\text{D2})$$

Note that the expression for the (minimal coupling gauge) Rabi frequency $\bar{\Omega}_R$ suggested in Ref. 25 is oversimplified. It does not contain factor $(\omega_{21}/\varpi_{n_{\min}})^{1/2}$.

The eigenvalue equation (D1) predicts the blueshift of the bare cavity photon frequency from $\varpi_{n_{\min}}$ to $\hat{\omega}_{n_{\min}}$. It is due to the presence of the diamagnetic (containing \mathbf{A}^2) term in the (one-electron) minimal coupling Hamiltonian.²⁵ In other words, omission of the diamagnetic term implies

the replacement $\hat{\omega}_{n_{\min}} \rightarrow \varpi_{n_{\min}}$ in the one-electron eigenvalue equation Eq. (D1). One can check that the above mentioned replacement is equivalent to the replacement $N_s \rightarrow N_s \omega_{12}^2 / \omega^2$ derived in Appendix B employing the semiclassical approach.

One also can check that making in Eq. (D1) the substitution $\omega_{21} \rightarrow \omega_{C_{n_{\min}}^{\text{inter}}}$ we practically reproduce semiclassical eigenvalue equation (17), which includes the intra- and interwell Coulomb coupling. It is worth stressing that the above mentioned substitution reproduces exactly the semiclassical result only when we take $f_{12} = 1$. It can be mainly associated with the fact that calculating the effect of the diamagnetic term the authors of Ref. 25 have assumed that all the oscillator strength is concentrated on the $1 \rightarrow 2$ transition ($f_{12} = 1$). On the other hand including the diamagnetic term in semiclassical approach we have restricted to the two subband approximation.

The inspection of Eqs. (D1) and (17) [see also Eq. (D3)] indicates that in the case uniform systems the interwell coupling partially compensates for the effects introduced by the diamagnetic term. The relative strength of the interwell coupling in the above mentioned systems is controlled by factor F defined by Eq. (16). Modeling the confining potential of the QW by the infinite square well of the width L_{QW} , one finds that expression for this factor can be written as $F \cong 0.58 L_{\text{QW}} / d_{\text{MQW}}$. The above result [see also Eq. (14)] is consistent with the statement that in typical systems the intrawell coupling plays a dominant role. Nevertheless, the effects connected with interwell coupling should be also considered, particularly when system enters into the USC regime. The authors of the recently published paper²⁸ claim that the effects connected with electron-electron interactions can be incorporated making the substitution $\omega_{21} \rightarrow \omega_{\text{IT}}$ in the (one-electron) minimal-coupling Hamiltonian, with the simultaneous replacement of single-particle operators by appropriate plasmonic operators. The above discussion indicates that such a substitution completely omits the effects connected with interwell coupling. It leads to substantial underestimation of the polariton branches blueshift in systems exhibiting the USC. To properly include the intra- and interwell Coulomb coupling, the following replacement $\omega_{21} \rightarrow \omega_{C_{n_{\min}}^{\text{inter}}}(k_x)$ should be used. The above conclusion seems to be consistent with the quantum-mechanical results reported in Ref. 26.

It is also instructive to discuss the case when the confining potential of the QW has a parabolic shape. Then all intrawell electron-electron interactions, including the depolarization shift, exactly cancel each other and the Q2DEG absorbs radiation only at the bare harmonic oscillator frequency which coincides with the bare subband separation $\omega_{21|N_s=0}$.^{8,10} Making the substitution $\omega_{\text{IT}} \rightarrow \omega_{21} \equiv \omega_{21|N_s=0}$ in Eq. (A4) for $\sigma_{zz}(\omega)$, one finds that the eigenvalue equation (17) for the polariton branches supported by model I with parabolic QWs reduces to the form

$$(\omega^2 - \omega_{21}^2)(\omega^2 - \varpi_{n_{\min}}^2) = 4\omega_{21}\varpi_{n_{\min}}\check{\Omega}_R^2, \quad (\text{D3})$$

where $\check{\Omega}_R = (\omega_p/2)(\varpi_{n_{\min}}/\omega_{21})^{1/2} \sin \theta_{n_{\min}}$ can be treated as the (dipolar gauge) Rabi coupling frequency in the case of parabolic QWs. Writing the above equation we have employed

fact that in the presently considered system $f_{12} = 1$ and consequently $F^{1/2}\omega_p = \omega_p$.

Making the substitution $c \rightarrow \infty$ in the above equation, one finds that the frequency of the intersubband Coulomb mode supported by model I with parabolic QWs is given by

$$\omega_{C_{n_{\min}}^{\text{inter}}} = \sqrt{\omega_{21}^2 - \omega_p^2 \sin^2 \theta_{n_{\min}}}. \quad (\text{D4})$$

The inspection of Eqs. (D3) and (D4) shows that, in agreement with the experimental results reported in Ref. 10, the polariton gap occurs also in the case of parabolic QWs. The gap is located between $\omega = \omega_{21}$ and $\omega = (\omega_{21}^2 - \omega_p^2)^{1/2}$. It is consistent with our previous statement that the appearance of the polariton gap is connected with the presence of the long-range interwell Coulomb coupling.

The numerical calculations are performed for the cavity (having dielectric mirrors, $n_{\min} = 1$) resonant with bar intersubband transitions $\omega_{21} = \varpi_1(k_x)$. We take $F = 0.6$ and $\omega_{\perp} = 0.3\omega_{21}$. The thick solid curves in Fig. 11 display the ω_p -dependence of the LPB and the UPB predicted by the exact Eq. (17), which takes into account the intra- and interwell (dynamic) Coulomb couplings. The frequency of the corresponding Coulomb mode $\omega_{C_{n_{\min}}^{\text{inter}}}$ resulting from Eq. (14) represents black dashed curve. (We neglect the shift of ω_{21} resulting from static charge effect.) The thin solid curves display the ω_p dependence of the polariton branches obtained employing the one-electron eigenvalue equation (D1). For comparison we also present (gray solid curves) the behavior of the polariton branches predicted by Eq. (D3), which takes into account only the interwell coupling. The corresponding Coulomb mode $\omega_{C_{n_{\min}}^{\text{inter}}}$, obtained employing Eq. (D4), is represented by the gray dashed curve.

The displayed results illustrate our previous statement that in typical systems the intrawell coupling plays a dominant role. This coupling leads to the blue shift of the branches with respect to the one-electron results (represented by the thin black solid curves). The above mentioned blue shift is partially reduced by the interwell coupling. It is obvious that the situation will be different in the case of the parabolic QWs where only the interwell coupling can be considered. Figure 11 shows [in agreement with Fig. 1(a) in Ref. 10] that the above mentioned coupling induces the redshift of the branches (represented by the gray solid curves) with respect to the one-electron results.

It is worth noting that the formula (D3), which was derived for planar systems, very well describes the experimental results reported by Geiser *et al.*¹⁰ for the MQW embedded into a microcavity based on an LC electronic resonator. We have checked that Eq. (D3) practically reproduces the solid curves in Fig. 3(a) of the above mentioned paper.

APPENDIX E: MODEL I. THE φ -DEPENDENT CHARACTERISTICS

For the sake of completeness, in this Appendix, we very briefly discuss the behavior of the polariton branches on the ω - φ plane. The φ dependence of the polariton branches can be obtained formally eliminating k_x from Eq. (13) with the help of the relation $k_x = K_w \sin \varphi$. (We assume for convenience

that $\varepsilon_s = \varepsilon_w$.) Performing appropriate manipulations, we get

$$\omega^2 - \check{\omega}_n^2 = \frac{F\omega_p^2\omega_{\Gamma}^2 \tan^2 \varphi}{\omega^2 - \omega_{\Gamma}^2} + \frac{\omega_p^2 n^2 \omega_{\perp}^2 \cos^{-2} \varphi}{\omega^2 - \omega_p^2}, \quad (\text{E1})$$

where $\check{\omega}_n^2(\varphi) = \underline{\omega}_n^2(\varphi) + F\omega_p^2 \tan^2 \varphi$. Note that Eq. (E1) describes the polariton modes located only within the light cone. They are accessible by the reflectance provided that we allow for the finite transmissivity of the coupling mirror.

In the absence of the intrasubband excitation, Eq. (E1) reduces to the form discussed in our previous papers:^{4,5}

$$(\omega^2 - \omega_{\Gamma}^2)(\omega^2 - \check{\omega}_n^2) = F\omega_p^2\omega_{\Gamma}^2 \tan^2 \varphi. \quad (\text{E2})$$

Let us discuss the limiting case when (i) mirrors are of a dielectric type, (ii) φ is close to φ_{res} and (iii) the RWA is valid, i.e., we assume that $\omega_{\Gamma}^2 \gg F(\omega_p/2)^2 \tan^2 \varphi_{\text{res}} \equiv \Omega_{\text{res}}^2$. In the considered limit, Eq. (E2) can be approximated and recast in the form $(\omega - \underline{\omega}_1)(\omega - \omega_{\Gamma}) = \Omega_{\text{res}}^2$ corresponding to the model of two-coupled oscillators [see Eq. (39)]. The polariton branches resulting from the above simplified equation are shifted with respect to the ‘‘exact’’ result predicted by Eq. (E2). Moreover, the minimal value of the branch splitting resulting from Eq. (E2) appears not at $\varphi = \varphi_{\text{res}}$, as it is suggested by the two coupled-oscillator expression, but at the angle $\varphi = \hat{\varphi}_{\text{res}}$, which is smaller than φ_{res} . The difference between φ_{res} and $\hat{\varphi}_{\text{res}}$ increases with increasing the ratio $\Omega_{\text{res}}/\omega_{\Gamma}$.

We have checked (results are not presented) that the modifications of the ICP dispersion induced by the intrasubband excitation are more strongly pronounced on the ω - φ plane than on the ω - k_x plane. For example, in the case of the system discussed in Fig. 1, the intrasubband plasmon induced blue shift of the LPB (at $\varphi_{\text{res}} = \theta_{\text{res}}$) is above five times larger on the ω - φ plane than on the ω - k_x plane.

APPENDIX F: RELATIONS USED FOR DERIVING EQ. (26)

$$\tan(h) \frac{\pi x}{2} = \frac{4x}{\pi} \sum_{k=1}^{\infty} \frac{1}{(2k-1)^2 - (+)x^2}, \quad (\text{F1})$$

$$\cot(h) \frac{\pi x}{2} = \frac{2}{\pi x} + \frac{4x}{\pi} \sum_{k=1}^{\infty} \frac{1}{(2k)^2 - (+)x^2}. \quad (\text{F2})$$

APPENDIX G: MICROCAVITY WITH SEMI-INFINITE PLASMONIC CLADDINGS

Below we discuss the electromagnetic modes supported by a microcavity consisting of a dielectric spacer (with thickness L_{MC} and the dielectric constant $\varepsilon_{\text{sl}} = \varepsilon_w$) bounded by semi-infinite n -doped dielectric claddings described by Drude-like dielectric function

$$\varepsilon_{\text{mirr}}(\omega) = \varepsilon_w(1 - \omega_p^2/\omega^2), \quad (\text{G1})$$

where $\omega_{p,\text{mirr}} = (4\pi N_D e^2/m^* \varepsilon_w)^{1/2}$ is the plasma frequency of the mirror material, N_D is the mirror material doping density. One can check that for N_D ranging from 10^{18} to 10^{19} cm^{-3} the plasma frequency $\omega_{p,\text{mirr}}$ can vary from 43.5 to 137.5 meV/ \hbar for $\varepsilon_w = \varepsilon_{\text{GaAs}} = 10.9$.

The electromagnetic modes supported by the considered system are the solutions of the following equation:^{30,35,61}

$$\tanh(\alpha_w L_{\text{MC}}/2) = -(\varepsilon_w \alpha_{\text{mirr}}/\varepsilon_{\text{mirr}} \alpha_w)^{\pm 1}, \quad (\text{G2})$$

where $\alpha_{\text{mirr}} = \sqrt{k_x^2 - \varepsilon_{\text{mirr}} \omega^2/c^2}$ and the \pm signs correspond to the symmetric and antisymmetric modes, respectively.

The modes, which are confined to the dielectric slab, exist only below the mirror boundary curve $\alpha_{\text{mirr}} = 0$. The area under the boundary curve ($\omega = \sqrt{\omega_{p,\text{mirr}}^2 + \omega_{\parallel}^2}$) can be divided into two regions denoted by \mathcal{V} and \mathcal{S} . Region \mathcal{V} (\mathcal{S}) is located within (outside) the spacer light cone. In region \mathcal{V} (\mathcal{S}), the quantity α_w is imaginary (real). The eigenmode can be treated as a volume mode when it is located in region \mathcal{V} or surface mode when located in region \mathcal{S} . The essential difference, compared to the case of perfect dielectric mirrors (discussed in Sec. III A) is the formation of the additional [one symmetric (S_{SP}) and one antisymmetric (A_{SP})] plasmonic modes.³⁰ The S_{SP} mode is located in region \mathcal{V} . It starts linearly at ($k_x = 0$, $\omega = 0$) and goes asymptotically towards the surface plasmon frequency $\omega_{p,\text{mirr}}^{\text{surf}} = \omega_{p,\text{mirr}}/2$ as $k_x \rightarrow \infty$. The A_{SP} mode starts at $k_x = 0$ and $\omega = \omega_{A_{\text{SP}}}^* < \omega_{p,\text{mirr}}$ as a volume mode. It crosses the line $\alpha_w = 0$, i.e., it changes its character into a surface type mode and goes asymptotically towards $\omega_{p,\text{mirr}}^{\text{surf}}$ as $k_x \rightarrow \infty$. The frequency $\omega_{A_{\text{SP}}}^*$ decreases with increasing L_{MC} . When the dielectric layer is sufficiently thin $\omega_{\perp}/2 > \omega_{p,\text{mirr}}^{\text{surf}}$ then the frequency $\omega_{A_{\text{SP}}}^*$ is located between $\omega_{p,\text{mirr}}^{\text{surf}}$ and $\omega_{p,\text{mirr}}$. In such systems, the A_{SP} mode has a negative dispersion at small k_x and exhibits a minimum.³¹ Except the above mentioned surface plasmonic modes, the system also supports volume ($c_{n \geq 1}$) photonic type modes. However, unlike in the case of perfect mirrors, the total number of the modes N_{tot} is finite and decreases with decreasing the ratio $\omega_{p,\text{mirr}}/\omega_{\perp}$. In the limiting case $\omega_{p,\text{mirr}}/\omega_{\perp} < 2$, the system supports only three modes ($N_{\text{tot}} = 3$): two surface plasmonic modes (S_{SP} and A_{SP}) and one photonic mode (c_1).

The replacement of the plasmonic mirrors by perfect metallic mirrors is equivalent to the substitution $\omega_{p,\text{mirr}} \rightarrow \infty$. Then, mode S_{SP} (A_{SP}) transforms into c_0 (c_1) photonic mode (see Sec. III A).

It is also instructive to consider the case when a strongly dispersive cladding material is replaced by a nondispersive dielectric material with a dielectric function $\varepsilon_c < \varepsilon_w$. It is obvious that the surface modes S_{SP} and A_{SP} do not survive the above mentioned replacement. In the system of interest here the photonic modes, confined to the dielectric slab, exist only between lines $\alpha_c = 0$ and $\alpha_w = 0$. More precisely, they start at line $\alpha_c = 0$ and go asymptotically to line $\alpha_w = 0$. It is interesting to note that, in contrast with the system with perfect dielectric mirrors, the lowest mode (c_1) starts at $k_x = 0$ and $\omega = 0$. This mode always exists. Its properties (at k_x close to 0) are similar to the properties of mode TM_0 .

When we replace the dielectric spacer by the MQW slab, Eq. (G2) transforms into the form

$$\tanh(\alpha_{\text{MQW}} L_{\text{MC}}/2) = -(\varepsilon_{xx} \alpha_{\text{mirr}}/\varepsilon_{\text{mirr}} \alpha_{\text{MQW}})^{\pm 1}, \quad (\text{G3})$$

where $\alpha_{\text{MQW}} \equiv -ik_{\text{MQW},z}$.

The solutions of the above equation describe the hybrid polariton modes resulting from the coupling of the (photonic/plasmonic) cavity modes with intersubband and

intrasubband excitations. The case when only intrasubband plasmons are coupled to the cavity photonic (plasmonic) modes has been discussed in Ref. 61 (Ref. 30).

APPENDIX H: MODE STRUCTURE OF MULTILAYER PLASMONIC MIRRORS

In order to understand the nature of the mode structure of the multilayer plasmonic mirror employed by Anappara *et al.*,⁶ we discuss a simple highest-symmetry structure. It consists of two n^+ dielectric plates, with thickness d_{n^+} and dielectric function $\varepsilon_{\text{mirr}}$ [see Eq. (G1)], separated by the distance L_{gap} and surrounded by undoped dielectric (ε_w).

The considered system can support four surface plasmon polariton (SPP) modes located below $\omega_{p,\text{mirr}}$. They appear due

to the coupling between the SPP modes supported by individual interfaces.^{62,63} In Ref. 63, the above mentioned modes are labeled S_L , A_L , S_H , and A_H according to their mode profiles. Labels S/A denote the symmetric/antisymmetric modes. Subscript letters L/H associate the mode as originated from the low/high energy branch of the single n^+ plate. The three lowest energy modes (S_L , A_L , S_H) always lie outside the light cone, i.e., they remain nonradiative. The highest mode (A_H) starts at $k_x = 0$ at finite frequency $\omega = \omega_{A_H}^* < \omega_{p,\text{mirr}}$ and crosses the light line (at $k_x = k_{A_H}^*$). The frequency $\omega_{A_H}^*$ decreases with increasing L_{gap} . Thus the above mentioned mode has a radiative character for $k_x < k_{A_H}^*$. The frequencies of all the four modes approach $\omega_{p,\text{mirr}}^{\text{surf}}$ at larger k_x . In the limit $d_{n^+} \rightarrow \infty$, the modes S_L and A_H transform into the modes S_{AP} and A_{SP} discussed in the previous Appendix.

APPENDIX I: LIST OF ACRONYMS AND IMPORTANT SYMBOLS

DBR	Distributed Bragg reflector
EMA	Effective medium approximation
ICP	Intersubband-cavity-polariton
LPB	Lower polariton branch
LWA	Long-wavelength approximation
MC	Microcavity
MQW	Multiple-quantum-well
Q2DEG	Quasi-2D-electron gas
SPP	Surface plasmon polariton
SSC	Super-strong coupling
TMF	Transfer matrix formalism
UPB	Upper polariton branch
USC	Ultra-strong coupling
d_{MQW}	Spatial period of the MQW
f_{12}	Oscillator strength of the intersubband transition
k_x	In-plane wave vector
k_x^{res}	In-plane wave vector at which the ground cavity mode is resonant with the intersubband transition
$k_{j(\text{MQW}),z}$	Normal component of the wave vector in the j th medium (MQW slab)
$L_{\text{MQW}(\text{MC})}$	Thickness of the MQW slab (MC)
$L_{\text{QW}}^{\text{eff}}$	Effective thickness of the QW
n	Mode index
n_{min}	Ground photonic mode index of the MC with metallic ($n_{\text{min}} = 0$) or dielectric ($n_{\text{min}} = 1$) mirrors
N_s	Surface electron density
$r_{c(b)}$	Reflection coefficient of the coupling (back) mirror
$\gamma_{\kappa(\text{IT})}$	Dephasing rate of the κ th mode (intersubband transition)
Δ_{CM}	Frequency separation between the two lowest cavity modes
$\Delta_{\text{ICP}} (\Delta_{\text{ICP}})$	Frequency separation between the UPB and LPB on the ω - k_x (ω - φ) plane
ε_j	Dielectric constant of the j th medium
$\varepsilon_{\text{mirr}}$	Dielectric function of the plasmonic mirror
$\varepsilon_{\rho\rho}$	Principal components of the MQW effective dielectric tensor ($\rho = x, y, z$)
$\sigma_{\rho\rho}$	Principal components of the sheet conductivity tensor
φ	Light propagation angle in the substrate
$\omega_{C_n^{\text{inter}}} (C_n^{\text{intra}})$	Frequency of the n -th intersubband (intrasubband) Coulomb mode supported by model I
$\omega_{C^{\text{inter}}}$	Frequency of the intrasubband Coulomb mode supported by model II
ω_{IT}	Frequency of the intersubband excitation supported by the QW
$\tilde{\omega}_{\kappa}$	Complex frequency of the κ th mode: $\tilde{\omega}_{\kappa} = \omega'_{\kappa} + i\omega''_{\kappa} = \omega'_{\kappa} - i\gamma_{\kappa}$
ω_n	Frequency of the n th photonic mode supported by model I
$\omega_{P(p)}$	Plasma frequency of the QW (bulk MQW)
$\omega_{p,\text{mirr}}$	Plasma frequency of the mirror material
$\Omega_R (\Omega_R^{\text{res}})$	Rabi frequency (Rabi frequency at $k_x = k_x^{\text{res}}$)

- ¹D. Dini, R. Kohler, A. Tredicucci, G. Biasiol, and L. Sorba, *Phys. Rev. Lett.* **90**, 116401 (2003).
- ²E. Dupont, H. C. Liu, A. J. Spring Thorpe, W. Lai, and M. Extavour, *Phys. Rev. B* **68**, 245320 (2003).
- ³A. A. Anappara, A. Tredicucci, F. Beltram, G. Biasiol, L. Sorba, S. De Liberato, and C. Ciuti, *Appl. Phys. Lett.* **91**, 231118 (2007).
- ⁴M. Załuźny and W. Zietkowski, *Phys. Rev. B* **78**, 033305 (2008).
- ⁵M. Załuźny and W. Zietkowski, *Phys. Rev. B* **80**, 245301 (2009).
- ⁶A. A. Anappara, S. De Liberato, A. Tredicucci, C. Ciuti, G. Biasiol, L. Sorba, and F. Beltram, *Phys. Rev. B* **79**, 201303(R) (2009).
- ⁷Y. Todorov, A. M. Andrews, R. Colombelli, S. De Liberato, C. Ciuti, P. Klang, G. Strasser, and C. Sirtori, *Phys. Rev. Lett.* **105**, 196402 (2010).
- ⁸A. Delteil, A. Vasanelli, Y. Todorov, C. Feuillet Palma, M. Renaudat St-Jean, G. Beaudoin, I. Sagnes, and C. Sirtori, *Phys. Rev. Lett.* **109**, 246808 (2012).
- ⁹B. Askenazi, A. Delteil, A. Vasanelli, Y. Todorov, G. Beaudoin, I. Sagnes, and C. Sirtori, in *Proceedings of 16th International Conference on Modulated Semiconductors, Wroclaw, 2013* (unpublished).
- ¹⁰M. Geiser, F. Castellano, G. Scalari, M. Beck, L. Nevou, and J. Faist, *Phys. Rev. Lett.* **108**, 106402 (2012).
- ¹¹J. Plumridge, E. Clark, R. Murray, and C. Phillips, *Solid Stat. Commun.* **146**, 406 (2008).
- ¹²G. Günter, A. A. Anappara, J. Hess, A. Sell, A. Biasiol, L. Sorba, S. De Liberato, C. Ciuti, A. Tredicucci, A. Leitenstorfer, and R. Huber, *Nature (London)* **458**, 157 (2009).
- ¹³M. Porer, J.M. Menard, A. Leitenstorfer, R. Huber, R. DeglInnocenti, S. Zanotto, G. Biasiol, L. Sorba, and A. Tredicucci, *Phys. Rev. B* **85**, 081302 (2012).
- ¹⁴E. Dupont, J. A. Gupta, and H. C. Liu, *Phys. Rev. B* **75**, 205325 (2007).
- ¹⁵D. Meiser and P. Meystre, *Phys. Rev. A* **74**, 065801 (2006).
- ¹⁶Y. Zhu, D. J. Gauthier, S. E. Morin, Q. Wu, H. J. Carmichael, and T. W. Mossberg, *Phys. Rev. Lett.* **64**, 2499 (1990).
- ¹⁷S. De Liberato and C. Ciuti, *Phys. Rev. B* **79**, 075317 (2009).
- ¹⁸L. Sapienza, A. Vasanelli, R. Colombelli, C. Ciuti, Y. Chassagneux, C. Manquest, U. Gennser, and C. Sirtori, *Phys. Rev. Lett.* **100**, 136806 (2008).
- ¹⁹Y. Todorov, P. Jouy, A. Vasanelli, L. Sapienza, R. Colombelli, U. Gennser, and C. Sirtori, *Appl. Phys. Lett.* **93**, 171105 (2008).
- ²⁰P. Jouy, A. Vasanelli, Y. Todorov, L. Sapienza, R. Colombelli, U. Gennser, and C. Sirtori, *Phys. Rev. B* **82**, 045322 (2010).
- ²¹A. Delteil, A. Vasanelli, P. Jouy, D. Barate, J. C. Moreno, R. Teissier, A. N. Baranov, and C. Sirtori, *Phys. Rev. B* **83**, 081404(R) (2011).
- ²²V. Agranovich, H. Benisty, and C. Weisbuch, *Solid. Stat. Commun.* **102**, 631 (1997).
- ²³V. Savona, *Lect. Notes Phys.* **531**, 173 (1999).
- ²⁴M. Richard, R. Romestain, R. Andre, and L. S. Dang, *Appl. Phys. Lett.* **86**, 071916 (2005).
- ²⁵C. Ciuti, G. Bastard, and I. Carusotto, *Phys. Rev. B* **72**, 115303 (2005).
- ²⁶Y. Todorov and C. Sirtori, *Phys. Rev. B* **85**, 045304 (2012).
- ²⁷Y. Todorov, L. Toso, A. Delteil, A. Vasanelli, C. Sirtori, A. M. Andrews, and G. Strasser, *Phys. Rev. B* **86**, 125314 (2012).
- ²⁸A. Auer and G. Burkard, *Phys. Rev. B* **85**, 235140 (2012).
- ²⁹L. I. Deych, *Phys. Rev. Lett.* **95**, 043902 (2005).
- ³⁰A. A. Bogdanov and R. A. Suris, *Phys. Rev. B* **83**, 125316 (2011).
- ³¹M. Litinskaya and V. M. Agranovich, *J. Phys. Condens Matter* **24**, 015302 (2012).
- ³²S. Hayashi, Y. Ishigaki, and M. Fujii, *Phys. Rev. B* **86**, 045408 (2012).
- ³³A. C. Tselis and J. J. Quinn, *Phys. Rev. B* **29**, 3318 (1984).
- ³⁴S. Das Sarma, *Phys. Rev. B* **29**, 2334 (1984).
- ³⁵J. Plumridge and Ch. Phillips, *Phys. Rev. B* **76**, 075326 (2007).
- ³⁶J. R. Plumridge, R. J. Steed, and C. C. Phillips, *Phys. Rev. B* **77**, 205428 (2008).
- ³⁷K. Y. Yang, V. Giannini, A. O. Bak, H. Amrania, S. A. Maier, and C. C. Phillips, *Phys. Rev. B* **86**, 075309 (2012).
- ³⁸M. Załuźny and C. Nalewajko, *Phys. Rev. B* **59**, 13043 (1999).
- ³⁹R. D. King-Smith and J. C. Inkson, *Phys. Rev. B* **36**, 4796 (1987).
- ⁴⁰A. Liu, *Phys. Rev. B* **55**, 7101 (1997).
- ⁴¹M. Kira, F. Jahnke, W. Hoyer, and S. W. Koch, *Prog. Quantum. Electron.* **23**, 189 (1999).
- ⁴²A. M. Stewart, *J. Mat. Struc.- Theochem* **626**, 47 (2003), and references therein.
- ⁴³K. Cho, *Reconstruction of Microscopic Maxwell Equations: A Single Susceptibility Theory* (Springer, Berlin Heidelberg, 2010).
- ⁴⁴O. Keller, *J. Opt. Soc. Am. B* **12**, 997 (1995).
- ⁴⁵K. L. Kliewer and R. Fuchs, *Phys. Rev.* **150**, 573 (1966).
- ⁴⁶A. Archambault, T. V. Teperik, F. Marquier, and J. J. Greffet, *Phys. Rev. B* **79**, 195414 (2009).
- ⁴⁷J-G. Caputo, E. V. Kazantseva, L. Loukitch and A. I. Maimistov, *J. Phys. A: Math. Gen.* **42**, 165204 (2009).
- ⁴⁸A. Tredicucci, Y. Chen, V. Pellegrini, M. Börger, L. Sorba, F. Beltram, and F. Bassani, *Phys. Rev. Lett.* **75**, 3906 (1995).
- ⁴⁹M. Litinskaya and V. M. Agranovich, *J. Phys.: Condens. Matter* **21**, 415301 (2009).
- ⁵⁰N. P. Andion, A. P. C. Malbouisson, and A. Mattos Neto, *J. Phys. A: Math. Gen.* **34**, 3735 (2001).
- ⁵¹A. Vukics and P. Domokos, *Phys. Rev. A* **86**, 053807 (2012).
- ⁵²M. Załuźny, *Phys. Stat. Sol. (b)* **123**, K57 (1984).
- ⁵³L. Wendler and E. Kändler, *Phys. Stat. Sol. (b)* **177**, 9 (1993).
- ⁵⁴T. Shih, K. Reimann, M. Woerner, T. Elsaesser, I. Waldmüller, A. Knorr, R. Hey, and K. H. Ploog, *Phys. Rev. B* **72**, 195338 (2005).
- ⁵⁵K. Oimatsu, T. Iida, H. Nishimura, K. Ogawa, and T. Katsuyama, *J. Lumin.* **48**, 713 (1991).
- ⁵⁶V. Savona, Z. Hradil, A. Quattropani, and P. Schwendimann, *Phys. Rev. B* **49**, 8774 (1994).
- ⁵⁷A. Castanié and D. Felbacq, *Opt. Commun.* **285**, 3353 (2012).
- ⁵⁸G. Panzarini, C. Andreani, A. Armitage, D. Baxter, M. S. Skolnik, V. N. Astratov, J. S. Roberts, A. V. Kavokin, M. R. Vladimirova, and M. A. Kaliteevski, *Phys. Solid State* **41**, 1223 (1999).
- ⁵⁹W. L. Bloss, *J. Appl. Phys.* **66**, 3639 (1989).
- ⁶⁰A. Eguluz and A. A. Maradudin, *Ann. Phys. (USA)* **113**, 29 (1978).
- ⁶¹W. Wonneberger and R. Lamche, *J. Phys. Chem. Solids* **59**, 231 (1998).
- ⁶²G. I. Stegeman and J. J. Burke, *Appl. Phys. Lett.* **43**, 221 (1983).
- ⁶³J. Chen, G. A. Smolyakow, S. R. J. Brueck, and K. Malloy, *Opt. Express* **16**, 14902 (2008).